

BREAKUP REACTIONS OF DRIP LINE NUCLEI¹

R. Shyam and R. Chatterjee

*Saha Institute of Nuclear Physics, 1/AF Bidhan Nagar,
Kolkata 700064, India*

¹Lectures presented in the workshop on
“Nuclei at Extremes of Isospin and Mass”,
held at Toshali Sands, Puri,
March 11 – 22, 2003.

Contents

1	Introduction	3
2	Formal Theory of Breakup Reactions	4
2.1	The Transition matrix and distorted wave Born approximation (DWBA)	5
2.2	Post form DWBA T – matrix in quasi free limit	9
3	Breakup amplitudes in the post form DWBA	12
3.1	Pure Coulomb breakup	12
3.2	Full breakup amplitude	26
4	Postacceleration effects in the Coulomb breakup of neutron halo nuclei	32
5	Summary, Conclusions and Future Outlook	37

ABSTRACT

The formal theory of breakup reactions is reviewed. The direct breakup mechanism which is formulated within the framework of the post form distorted wave Born approximation is discussed in detail. In this theory, which requires the information about only the ground state wave function of the projectile, the fragment-target interactions are included to all orders while fragment-fragment interaction is treated only in the first order. The general applicability of this theory to describe the breakup of halo nuclei is demonstrated by comparing the calculations with data for total, as well as energy and angle integrated cross sections and momentum distributions of fragments in reactions induced by a number of halo nuclei. We investigate the role played by the pure Coulomb, pure nuclear and the Coulomb-nuclear interference terms. Postacceleration effects in the Coulomb breakup of neutron halo nuclei is also studied.

1 Introduction

Recently advances made in accelerator and related technologies have provided us the opportunity to produce and work with nuclei having very short half-lives and very small one- or two-nucleon separation energies [1-14]. These nuclei lie very close to drip lines (the limit of neutron or proton binding). Nuclei at extremes of binding can exhibit behaviours which are quite different from those of the stable isotopes. We still lack a fully microscopic understanding of the stability of these unique many body systems. These nuclei are important also from the nuclear astrophysics point of view. The rapid neutron capture (the r-process) together with the slow neutron capture (the s-process), which are dominant mechanisms for the nucleosynthesis of heavy elements above iron pass mostly through the neutron rich region. The properties of these nuclei are important inputs to theoretical calculations on stellar burning which otherwise are often forced to rely on global assumptions about nuclear masses, decays and level structures extracted from stable nuclei.

The first round of measurements involving neutron rich nuclei [15, 16, 17, 18, 19, 20] have confirmed the existence of a novel structure in some of them in which a low density tail of loosely bound neutrons extends too far out in the coordinate space as compared to a stable core (also known as the neutron halo¹). The quantum mechanical tunneling of very loosely bound valence neutrons leads to the formation of such a structure. The existence of neutron halo has been confirmed in ¹¹Be [22], ¹⁴B [23, 24], ¹⁹C [25] (one-neutron halo), and ⁶He, ¹¹Li [15, 26, 27], ¹⁴Be [28, 29], and ¹⁷B [28] (two-neutron halo). Recently, some proton halo nuclei have also been identified (⁸B [30, 31, 32], ¹⁷Ne [33], ²⁰Mg [34], and ^{26,27,28}P [35]).

Halo nuclei, in most cases, have only one bound state (the ground state) and a broad featureless continuum. Thus, methods of conventional nuclear structure studies, namely, measurements of energies and spin-parities of excited states are not applicable in these cases. However, due to their small binding energies, they can be easily excited above their particle emission thresholds. Hence their breakup reactions in the Coulomb and nuclear fields of the target nuclei could be useful tools to investigate their structures.

To be able to extract reliable structure information of halo nuclei from the breakup data, it is quite desirable to have a theory of these reactions which (1) is fully quantum mechanical; (2) treats the Coulomb and nuclear breakups as well as their interference terms consistently on an equal footing; (3) includes the recoil of the core within the halo nucleus, and the finite range of the core-halo interaction, and (4) involves least adjustable parameters.

We discuss the formal theory for halo breakup reactions in section 2. We specially mention a theory formulated within the framework of the post form distorted wave Born approximation (DWBA) where both Coulomb and nuclear breakups can be treated consistently on an equal footing. The full ground state

¹The term ‘neutron halo’ was introduced by Burhop et al. [21], in the context (now called ‘neutron skin’) of the bulk of the neutron density extending further out in space than the proton density.

wave function of the projectile enters as an input into this theory. Thus, information about the halo structure can be extracted by comparing the calculations with the available data. This is shown in section 3. We also discuss the role of nuclear breakup and of Coulomb-nuclear interference (CNI) terms in this section. The post form DWBA theory is uniquely suited to study the postacceleration effects in the halo breakup reactions. This is an higher order effect which is studied in section 4. We give conclusions and the future outlook in section 5.

2 Formal Theory of Breakup Reactions

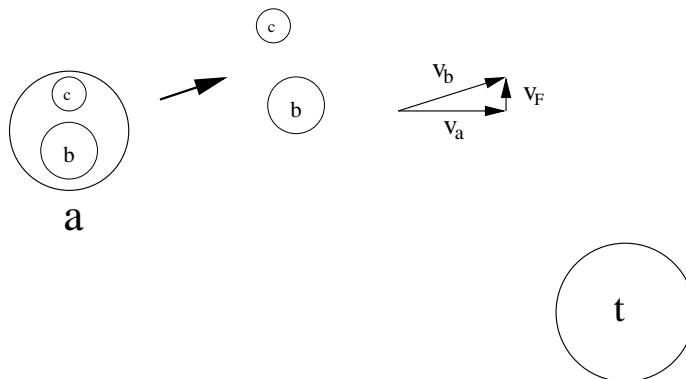


Figure 1: The direct breakup mechanism in a participant - spectator model.

The basic mechanism of the breakup reactions can be described in a simple participant-spectator model in which the projectile a which is supposed to consist of two substructures, say, b and c , interacts with a target t . It might so happen that one of the substructures b (the spectator) misses the target and keeps moving in its original direction while the substructure c (the participant) interacts with it. In such a situation the velocity of fragment b (\mathbf{v}_b) can be written as

$$\mathbf{v}_b = \mathbf{v}_a + \mathbf{v}_F, \quad (1)$$

where \mathbf{v}_a is the velocity of projectile a , and \mathbf{v}_F is the velocity associated with the Fermi motion of b inside the projectile before its breakup (see Fig. 1). Therefore

$$v_b^2 = v_a^2 + v_F^2 + 2\mathbf{v}_a \cdot \mathbf{v}_F. \quad (2)$$

As $v_F^2 \ll v_a^2$, we can neglect v_F^2 in Eq. (2) and get the maximum and minimum values of v_b^2 (corresponding to + and - signs, respectively) to be given by

$$v_b^2 \approx v_a^2 \pm 2v_a v_F. \quad (3)$$

Hence, maximum and minimum possible energies of b in the final channel are given by

$$E_b = \frac{1}{2}m_b v_b^2 = \frac{m_b}{m_a} \left(\frac{1}{2}m_a v_a^2 \pm m_a v_a v_F \right), \quad (4)$$

where m_b is the mass of fragment b , and m_a is the mass of the projectile a . Defining $p_a = m_a v_a$ and $p_F = m_b v_F$, we have

$$E_b = \frac{m_b}{m_a} E_a \pm \frac{p_a p_F}{m_a}. \quad (5)$$

Thus, in the energy spectrum of particle b one would expect a peak at $\frac{m_b}{m_a} E_a$, with a width $(2 \frac{p_a p_F}{m_a})$ depending on its Fermi momentum inside the projectile. This simple picture, which was proposed by Serber [36] way back in 1947, is realized remarkably well in majority of the breakup data.

Now, unless some kind of exclusive measurement is made in which both fragments b and c are detected, the fragment c can interact with the target nucleus, t , in all possible ways. We distinguish between two classes of breakup processes: elastic breakup, where the target nucleus remains in the ground state (the interaction $c-t$ is elastic) and inelastic breakup where c can interact in all possible ways with the target nucleus (inelastic excitation of the target, compound nucleus formation, transfer processes etc.).

There is another picture of breakup reactions in which the projectile is excited as a whole to a state in the continuum which subsequently decays into fragments b and c as it leaves the interaction zone. This process is called the sequential breakup (or resonant breakup). Both Coulomb and nuclear interactions between the projectile and target can cause the inelastic excitation of the former.

In the next sub-section, we shall describe the transition amplitude and its various representations and introduce the distorted wave Born approximation.

2.1 The Transition matrix and distorted wave Born approximation (DWBA)

Let us consider the reaction $a + t \rightarrow b + c + t$, in a three body model, where the projectile a , incident with momentum \mathbf{q}_a , breaks up into fragments b and c with momenta \mathbf{q}_b and \mathbf{q}_c , respectively in the Coulomb and nuclear fields of a target t .

The Hamiltonian of the system is written as

$$H = T_b + T_c + T_t + V_{bc} + V_{bt} + V_{ct}, \quad (6)$$

where T_i is the kinetic energy of particle i and V_{ij} is the two-body interaction between i and j ; their separation will be denoted by \mathbf{r}_{ij} in the following.

To find the interaction in the initial and final channels, we note that the asymptotic Hamiltonians in the initial (prior) and final (post) channels are

$$H_i = T_b + T_c + T_t + V_{bc} \quad (7)$$

and

$$H_f = T_b + T_c + T_t, \quad (8)$$

respectively. Hence the initial (prior) channel interaction is

$$V_i = H - H_i = V_{bt} + V_{ct} \quad (9)$$

and the final (post) channel interaction is

$$V_f = H - H_f = V_{bc} + V_{bt} + V_{ct}. \quad (10)$$

There are two exact T - matrices [37]

$$T_{fi}^{(+)[post]} = \langle e^{i\mathbf{q}_c \cdot \mathbf{r}_{ct}} e^{i\mathbf{q}_b \cdot \mathbf{r}_{bt}} | V_{bc} + V_{bt} + V_{ct} | \Psi_i^{(+)} \rangle, \quad (11)$$

and

$$T_{fi}^{(-)[prior]} = \langle \Psi_i^{(-)} | V_{bt} + V_{ct} | e^{i\mathbf{q}_a \cdot \mathbf{r}_{at}} \phi_a(\mathbf{r}_{bc}) \rangle, \quad (12)$$

which are the starting points for a discussion on the theory of breakup processes. The ground state wave function of the projectile, $\phi_a(\mathbf{r}_{bc})$, satisfies

$$(T_b + T_c + V_{bc})\phi_a(\mathbf{r}_{bc}) = -\epsilon_a \phi_a(\mathbf{r}_{bc}), \quad (13)$$

where ϵ_a is the separation energy between fragments b and c in the ground state of the projectile. $\Psi_i^{(+)}$ is the exact three-body scattering wave function with *outgoing wave* boundary condition (denoted by (+) sign in the superscript), and $\Psi_f^{(-)}$ is the exact three-body scattering wave function with *ingoing wave* boundary condition (denoted by (-) sign in the superscript). They are the exact eigenfunctions of the three-body Hamiltonian [Eq. (6)]. Thus they satisfy

$$H\Psi_i^{(+)} = E\Psi_i^{(+)} \quad (14)$$

and

$$H\Psi_f^{(-)} = E\Psi_f^{(-)}, \quad (15)$$

where E is the total energy of the system. We now use the Gell-Mann – Goldberger two potential formula [38] to rewrite Eqs. (11) and (12) as

$$T_{fi}^{(+)[post]} = \langle \chi_{q_c}^{(-)}(\mathbf{r}_{ct}) \chi_{q_b}^{(-)}(\mathbf{r}_{bt}) | V_{bc} + V_{bt} + V_{ct} - U_{bt} - U_{ct} | \Psi_i^{(+)} \rangle \quad (16)$$

and

$$T_{fi}^{(-)[prior]} = \langle \Psi_f^{(-)} | V_{ct} + V_{bt} - U_{at} | \chi_{q_a}^{(+)}(\mathbf{r}_{at}) \phi_a(\mathbf{r}_{bc}) \rangle. \quad (17)$$

In Eqs. (16) and (17), wave functions $\chi_{q_c}^{(-)}(\mathbf{r}_{ct}) \chi_{q_b}^{(-)}(\mathbf{r}_{bt})$ and $\chi_{q_a}^{(+)}(\mathbf{r}_{at})$ satisfy the Schrödinger equations

$$[T_{r_{ct}} + T_{r_{bt}} + U_{bt} + U_{ct}] \chi_{q_c}^{(-)}(\mathbf{r}_{ct}) \chi_{q_b}^{(-)}(\mathbf{r}_{bt}) = E \chi_{q_c}^{(-)}(\mathbf{r}_{ct}) \chi_{q_b}^{(-)}(\mathbf{r}_{bt}) \quad (18)$$

and

$$[T_{r_{at}} + U_{at}]\chi_{q_a}^{(+)}(\mathbf{r}_{at}) = (E + \epsilon_a)\chi_{q_a}^{(+)}(\mathbf{r}_{at}), \quad (19)$$

respectively. In Eqs. (18) and (19), U_{it} are auxiliary potentials acting between particle ‘ i ’ and the target.

Assuming $V_{bt} = U_{bt}$ and $V_{ct} = U_{ct}$ in Eq. (16), we have [39, 40]

$$T_{fi}^{(+)[post]} = \langle \chi_{q_c}^{(-)}(\mathbf{r}_{ct})\chi_{q_b}^{(-)}(\mathbf{r}_{bt})|V_{bc}|\Psi_i^{(+)}\rangle. \quad (20)$$

Let us now introduce the distorted wave Born Approximation (DWBA) [41] for the exact wave functions $\Psi_i^{(+)}$ and $\Psi_f^{(-)}$ in Eqs. (20) and (17).

If one assumes that the inelastic excitations of the projectile are small, then the wave function $\Psi_i^{(+)}$ can be approximated by

$$\Psi_i^{(+)} \approx \chi_{q_a}^{(+)}(\mathbf{r}_{at})\phi_a(\mathbf{r}_{bc}). \quad (21)$$

The post form DWBA T – matrix is then

$$T_{fi}^{(+)[post]}(DWBA) = \langle \chi_{q_b}^{(-)}(\mathbf{r}_{bt})\chi_{q_c}^{(-)}(\mathbf{r}_{ct})|V_{bc}|\chi_{q_a}^{(+)}(\mathbf{r}_{at})\phi_a(\mathbf{r}_{bc})\rangle. \quad (22)$$

If, on the other hand, one assumes that the final state interaction between the breakup fragments (b and c) is not important, i.e. V_{bc} is weak in the final channel, then one can write the exact wave function $\Psi_f^{(-)}$ as,

$$\Psi_f^{(-)} \approx \chi_{q_b}^{(-)}(\mathbf{r}_{bt})\chi_{q_c}^{(-)}(\mathbf{r}_{ct}). \quad (23)$$

This leads to the prior form DWBA T – matrix

$$T_{fi}^{(-)[prior]}(DWBA) = \langle \chi_{q_b}^{(-)}(\mathbf{r}_{bt})\chi_{q_c}^{(-)}(\mathbf{r}_{ct})|V_{ct} + V_{bt} - U_{at}|\chi_{q_a}^{(+)}(\mathbf{r}_{at})\phi_a(\mathbf{r}_{bc})\rangle. \quad (24)$$

It can be shown [42] that the DWBA T – matrices given by Eqs. (22) and (24) are equivalent to one another, i.e.,

$$T_{fi}^{(+)[post]}(DWBA) = T_{fi}^{(-)[prior]}(DWBA). \quad (25)$$

Thus, for actual calculations, one may use the T – matrix which seems more convenient. $T^{(-)[prior]}$ involves very complicated coordinate transformations as compared to the $T^{(+)[post]}$ form and hence it is very difficult to work with it in actual problems. Moreover V_{bc} in Eq. (22) is of a shorter range than $V_{ct} + V_{bt} - U_{at}$ in Eq. (24), which would make the numerical evaluation of Eq. (22) relatively easier. The post form DWBA has been extensively used to perform breakup calculations [37, 43, 44, 45].

However, by introducing a different approximation for $\Psi_f^{(-)}$ an alternate prior form T – matrix can be obtained. If we assume that the final state interaction V_{bc} between the fragments b and c is important, then one can approximate $\Psi_f^{(-)}$ as

$$\Psi_f^{(-)} \approx \chi_{\mathbf{Q}_f}^{(-)}(\mathbf{r}_{at})\phi_{a^*,\mathbf{q}_f}^{(-)}(\mathbf{r}_{bc}). \quad (26)$$

In Eq. (26), the relative motion wave function of b and c (which could also be a resonant state) is described by $\phi_{a^*,\mathbf{q}_f}^{(-)}(\mathbf{r}_{bc})$, where \mathbf{q}_f denotes the relative momentum between the fragments. The center of mass (c.m.) motion of the unbound system ($a^* = b + c$) with respect to the target in the final state is given by $\chi_{\mathbf{Q}_f}^{(-)}(\mathbf{r}_{at})$ with momentum \mathbf{Q}_f . They are related to momenta \mathbf{q}_b and \mathbf{q}_c of fragments b and c by

$$\mathbf{Q}_f = \mathbf{q}_b + \mathbf{q}_c \quad (27)$$

and

$$\mathbf{q}_f = \frac{m_b}{m_a}\mathbf{q}_b - \frac{m_c}{m_a}\mathbf{q}_c, \quad (28)$$

respectively.

This approximation [Eq. (26)] leads to an alternate prior form T – matrix

$$T_{fi}^{(-)[alt,prior]}(DWBA) = \langle \chi_{\mathbf{Q}_f}^{(-)}(\mathbf{r}_{at})\phi_{a^*,\mathbf{q}_f}^{(-)}(\mathbf{r}_{bc}) | V_{ct} + V_{bt} - U_{at} | \chi_{q_a}^{(+)}(\mathbf{r}_{at})\phi_a(\mathbf{r}_{bc}) \rangle \quad (29)$$

or

$$T_{fi}^{(-)[alt,prior]}(DWBA) = \langle \chi_{\mathbf{Q}_f}^{(-)}(\mathbf{r}_{at})\phi_{a^*,\mathbf{q}_f}^{(-)}(\mathbf{r}_{bc}) | V_{ct} + V_{bt} | \chi_{q_a}^{(+)}(\mathbf{r}_{at})\phi_a(\mathbf{r}_{bc}) \rangle. \quad (30)$$

In Eq. (29), U_{at} depends on \mathbf{r}_{at} while $\phi_{a^*,\mathbf{q}_f}^{(-)}(\mathbf{r}_{bc})$ and $\phi_a(\mathbf{r}_{bc})$ depends on \mathbf{r}_{bc} , and hence the explicit dependence on U_{at} in Eq. (30) has dropped out because of the orthogonality of $\phi_{a^*,\mathbf{q}_f}^{(-)}(\mathbf{r}_{bc})$ and $\phi_a(\mathbf{r}_{bc})$. We note that Eq. (30) contains only two distorted waves as against the three distorted waves in $T^{(+)[post]}$. The distorted waves being oscillatory even at large distances, any reduction in their number will accelerate the convergence of the T – matrix. The alternate prior form has been used for performing breakup calculations by several authors [46, 47]. It should be noted that $T_{fi}^{(-)[alt,prior]}(DWBA)$ is no longer equivalent to $T_{fi}^{(+)[post]}(DWBA)$.

The T – matrix [Eq. (30)] describes a situation in which the projectile a is inelastically excited from the ground state to its continuum. If we ignore the nuclear interactions in the distorted waves in both incident and final channels and also ignore the nuclear parts of interactions V_{ct} and V_{bt} , then the alternate prior form T – matrix describes the Coulomb excitation of the projectile. The semi-classical counterpart of Eq. (30) is the Alder–Winther theory of Coulomb excitation [48].

The alternate prior form DWBA can be regarded as the first iteration of the solutions of a coupled channels problem e.g., the coupled discretized continuum channels or CDCC equations (see, e.g. [51]). However breakup studies of both stable isotopes [49, 50] and halo nuclei [52, 53, 54] have shown that the alternate prior form DWBA is insufficient to describe the data and that higher order coupling effects of the breakup channels are important in both the cases.

In the next sub-section, we show that by suitably rewriting the post form DWBA T – matrix [Eq. (22)], the features of the spectator-participant mechanism can be explicitly seen therein [55].

2.2 Post form DWBA T – matrix in quasi free limit

In Eq. (22), we replace the relative motion wave function of the projectile by a plane wave, i.e.,

$$\chi_{q_a}^{(+)}(\mathbf{r}_{at}) = e^{i\mathbf{q}_a \cdot \mathbf{r}_{at}}, \quad (31)$$

and rewrite the scattering wave functions in the final state, in terms of the half off-shell t -matrix elements $[t_{jt}(\mathbf{p}, \mathbf{q}_j), E = p^2/2m_j]$ as,

$$\chi_{q_j}^{(-)}(\mathbf{r}_{jt}) = e^{i\mathbf{q}_j \cdot \mathbf{r}_{jt}} + \lim_{\epsilon \rightarrow 0} \frac{1}{(2\pi)^3} \int d^3p \frac{t_{jt}(\mathbf{p}, \mathbf{q}_j) e^{i\mathbf{p} \cdot \mathbf{r}_{jt}}}{p^2 - q_j^2 + i\epsilon}, \quad j = b, c. \quad (32)$$

The T – matrix then has four terms: (1) a term containing three plane waves, which vanishes because of energy conservation, (2) a term (T_c) describing the scattering of particle c on t ,

$$T_c = \frac{1}{(2\pi)^3} \lim_{\epsilon \rightarrow 0} \int \int \int d^3r_{bc} d^3r_{at} d^3p \frac{e^{-i\mathbf{p} \cdot \mathbf{r}_{ct}}}{p^2 - q_c^2 - i\epsilon} t_{ct}^*(\mathbf{p}, \mathbf{q}_c) e^{-i\mathbf{q}_b \cdot \mathbf{r}_{bt}} V_{bc}(r_{bc}) e^{i\mathbf{q}_a \cdot \mathbf{r}_{at}} \phi_a(\mathbf{r}_{bc}), \quad (33)$$

(3) a term (T_b) [which is similar to that given by Eq. (33)] describing the scattering of particle b on t , (4) and a term (T_{bc}) describing the scattering of both b and c on t (double scattering).

Let us consider, e.g., the term T_c [Eq. (33)]. We express \mathbf{r}_{ct} and \mathbf{r}_{bt} in terms of \mathbf{r}_{bc} and \mathbf{r}_{at} (Fig. 2) as,

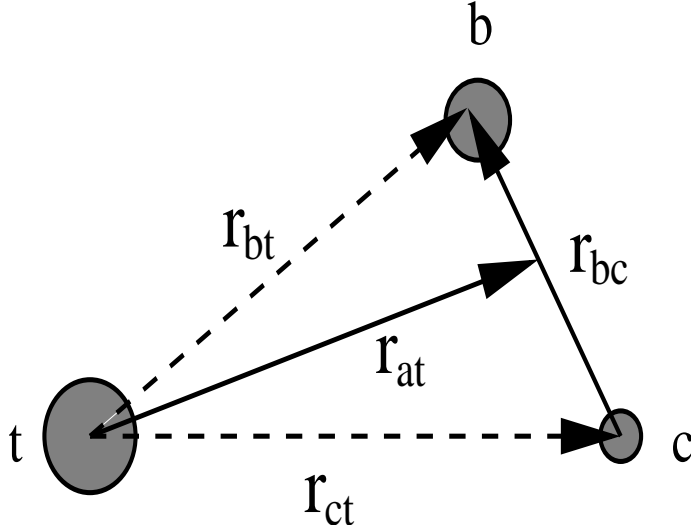


Figure 2: The coordinate system used in section 2.2.

$$\mathbf{r}_{ct} = \mathbf{r}_{at} - \frac{m_b}{m_a} \mathbf{r}_{bc} \quad (34)$$

and

$$\mathbf{r}_{bt} = \mathbf{r}_{at} + \frac{m_c}{m_a} \mathbf{r}_{bc}. \quad (35)$$

Substituting Eqs. (34) and (35) in Eq. (33) we get,

$$\begin{aligned} T_c &= \frac{1}{(2\pi)^3} \lim_{\epsilon \rightarrow 0} \int \int \int d^3 r_{bc} d^3 r_{at} d^3 p \frac{e^{i(\mathbf{q}_a - \mathbf{q}_b - \mathbf{p}) \cdot \mathbf{r}_{at}}}{p^2 - q_c^2 - i\epsilon} e^{i(\frac{m_b}{m_a} \mathbf{p} - \frac{m_c}{m_a} \mathbf{q}_b) \cdot \mathbf{r}_{bc}} t_{ct}^*(\mathbf{p}, \mathbf{q}_c) \\ &\times V_{bc}(r_{bc}) \phi_a(\mathbf{r}_{bc}) \end{aligned} \quad (36)$$

Integrations over coordinates \mathbf{r}_{at} and \mathbf{p} can be performed easily to give,

$$T_c = \frac{t_{ct}^*(\mathbf{q}_a - \mathbf{q}_b, \mathbf{q}_c)}{(\mathbf{q}_a - \mathbf{q}_b)^2 - q_c^2} F(\mathbf{Q}), \quad (37)$$

where

$$F(\mathbf{Q}) = \int d^3 r_{bc} e^{i\mathbf{Q} \cdot \mathbf{r}_{bc}} V_{bc}(r_{bc}) \phi_a(\mathbf{r}_{bc}), \quad (38)$$

with

$$\mathbf{Q} = \frac{m_b}{m_a} \mathbf{q}_a - \mathbf{q}_b. \quad (39)$$

Now the Schrödinger equation for the $b-c$ system can be used to rewrite Eq. (38) as

$$F(\mathbf{Q}) = -(2\pi)^{3/2} \frac{\hbar^2}{2\mu_{bc}} (\alpha^2 + Q^2) \tilde{\phi}_a(\mathbf{Q}), \quad (40)$$

where

$$\tilde{\phi}_a(\mathbf{Q}) = (2\pi)^{-3/2} \int d^3 r_{bc} e^{i\mathbf{Q} \cdot \mathbf{r}_{bc}} \phi_a(\mathbf{r}_{bc}) \quad (41)$$

is the momentum space wave function of the projectile in its ground state. In Eq. (40) α is defined as

$$\epsilon_{bc} = \frac{\hbar^2 \alpha^2}{2\mu_{bc}}, \quad (42)$$

where ϵ is the binding energy of the $b-c$ system and μ_{bc} is the corresponding reduced mass. Thus T_c is written as

$$T_c = -(2\pi)^{3/2} \frac{\hbar^2}{2\mu_{bc}} \frac{t_{ct}^*(\mathbf{q}_a - \mathbf{q}_b, \mathbf{q}_c)}{(\mathbf{q}_a - \mathbf{q}_b)^2 - q_c^2} (\alpha^2 + Q^2) \tilde{\phi}_a(\mathbf{Q}). \quad (43)$$

Now, for an infinitely heavy target, the energy conservation gives

$$-\frac{(\alpha^2 + Q^2)}{(\mathbf{q}_a - \mathbf{q}_b)^2 - q_c^2} = \frac{m_b}{m_a}. \quad (44)$$

Substituting Eq. (44) in Eq. (43) we obtain,

$$T_c = \frac{\hbar^2}{2m_c} (2\pi)^{3/2} t_{ct}^*(\mathbf{q}_a - \mathbf{q}_b, \mathbf{q}_c) \tilde{\phi}_a(\mathbf{Q}). \quad (45)$$

A similar expression holds for T_b .

If the off-shell dependence of $t_{ct}^*(\mathbf{q}_a - \mathbf{q}_b, \mathbf{q}_c)$ in Eq. (45), is neglected [55], then the breakup cross section is determined by the modulus square of the wave function, $\tilde{\phi}_a(\mathbf{Q})$. The maximum cross section would occur when

$$\mathbf{Q} = \frac{m_b}{m_a} \mathbf{q}_a - \mathbf{q}_b = 0, \quad (46)$$

or

$$\mathbf{v}_a = \mathbf{v}_b, \quad (47)$$

i.e., when particle b moves with the beam velocity and is only a ‘spectator’ in the breakup process. Thus, the term T_c (or T_b) has the simple physical interpretation: particle c (or b) interacts with t via V_{ct} (or V_{bt}) and is knocked out of the projectile, while particle b (or c) is only a spectator. This shows that the main feature of the Serber model – the dependence of the cross section on the internal momentum distribution of the fragment within the projectile – is embedded within the post form DWBA T – matrix in a quasi free limit.

It must, however, be cautioned that while some gross physical insights are obtained from the quasi free limit of the post form DWBA T – matrix, actual calculations must be made with full distorted waves [56] in order to explain the breakup data.

The breakup reactions of halo nuclei have been investigated by several authors using a variety of approaches (see, e.g., [57, 58, 59, 60], and [61], for an exhaustive bibliography on the subject). However, only a few [47, 62, 63, 64, 65] of them treat both Coulomb and nuclear breakup terms consistently on an equal footing. In Ref. [47] the prior form T – matrix given by Eq. (30) has been used to study the breakup reactions of ^8B . It should be recalled that in this T – matrix the fragment-target interaction is treated in first order which was subsequently shown to be inadequate. In Refs. [62, 65] the time evolution of the projectile in the coordinate space is described by solving the time dependent Schrödinger equation, treating the projectile target interaction as a time dependent external perturbation. These calculations use the semiclassical concept of the motion of the projectile along a trajectory.

The post form DWBA formulation of breakup reactions which uses the T matrix given by Eq. (20) includes consistently both Coulomb and nuclear interactions between the projectile fragments and the target nucleus to all orders,

but treats the fragment-fragment interaction in first order. As can be noted easily, the full wave function describing the ground state structure of the projectile, enters as an input in this theory which makes it possible to investigate the structure of the projectile from the study of the breakup reactions. It can treat the Coulomb and nuclear breakups as well as their interference terms consistently on an equal footing. Since this theory uses the post form scattering amplitude, the breakup contributions from the entire valence nucleon-core fragment continuum corresponding to all the multipoles and the relative angular momenta are included in it. This can account for the postacceleration effects in a unique way. In the subsequent sections we describe this theory in some details.

3 Breakup amplitudes in the post form DWBA

3.1 Pure Coulomb breakup

Coulomb dissociation of halo nuclei has been investigated by several authors using a number of different theoretical approaches. A semiclassical coupled channels formalism has been used by authors of Ref. [66], while in Refs. [67, 68] the time dependent Schrödinger equation method was employed. The results within these approaches depend on the range of the impact parameter associated with the straight line trajectories used to describe the motion of the projectile in the field of target nuclei. However, in these studies the emphasis was on investigating the dynamics of the Coulomb dissociation, and not the structure of the projectile ground state which was assumed to have some very simple zero range (ZR) form. Similar assumption for the projectile structure was also made in other semiclassical [69, 70] and prior form distorted wave Born approximation (DWBA) calculations [71].

In this section, we present a theoretical model to describe the pure Coulomb breakup of one-neutron halo nuclei within the framework of the post form DWBA where finite range effects are included via a local momentum approximation (LMA) [72, 73, 74]. This theory of breakup reactions incorporates the details of the ground state structure of the projectile in the breakup amplitude [37, 77].

We consider the reaction $a + t \rightarrow b + c + t$, where the projectile a breaks up into fragments b (charged) and c (uncharged) in the Coulomb field of a target t . The coordinate system chosen is shown in Fig. 3.

The position vectors satisfy the following relations

$$\mathbf{r} = \mathbf{r}_i - \alpha \mathbf{r}_1, \quad \alpha = \frac{m_c}{m_c + m_b} \quad (48)$$

$$\mathbf{r}_c = \gamma \mathbf{r}_1 + \delta \mathbf{r}_i, \quad \delta = \frac{m_t}{m_b + m_t}, \quad \gamma = (1 - \alpha\delta) \quad (49)$$

The starting point of our discussion is the post form DWBA T - matrix [Eq.

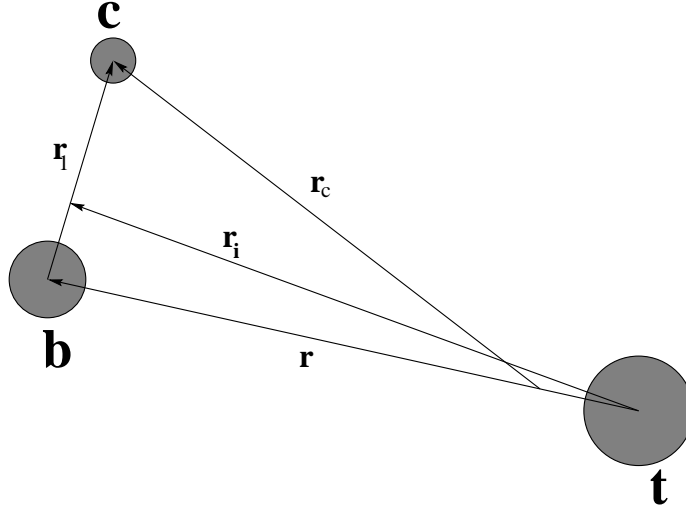


Figure 3: Coordinate system used in the T -matrix (Eq. 50). b , c and t represent the charged core, valence neutron and target, respectively.

(20)]

$$T = \int \int \int d\xi d\mathbf{r}_1 d\mathbf{r}_i \chi_b^{(-)*}(\mathbf{k}_b, \mathbf{r}) \Phi_b^*(\xi_b) \chi_c^{(-)*}(\mathbf{k}_c, \mathbf{r}_c) \Phi_c^*(\xi_c) V_{bc}(\mathbf{r}_1) \times \Phi_a(\xi_a, \mathbf{r}_1) \chi_a^{(+)}(\mathbf{k}_a, \mathbf{r}_i), \quad (50)$$

where χ 's are the distorted waves for relative motions of b and c with respect to t and the center of mass (c.m.) of the $b-t$ system, respectively, and Φ 's are the internal state wave functions of concerned particles with internal coordinates ξ . \mathbf{k}_b , \mathbf{k}_c are Jacobi wave vectors of b and c , respectively in the final channel of the reaction. $V_{bc}(\mathbf{r}_1)$ is the interaction between b and c . The charged fragment b and the projectile a interacts with the target by a point Coulomb interaction and hence the corresponding distorted waves are the Coulomb distorted waves with appropriate boundary conditions. For pure Coulomb breakup, the interaction between the target and uncharged fragment c is zero and hence for this case we can write $\chi_c^{(-)*}(\mathbf{k}_c, \mathbf{r}_c) = e^{-i(\mathbf{k}_c \cdot \mathbf{r}_c)}$. $\Phi_a(\xi_a, \mathbf{r}_1)$ represents the bound state wave function of the projectile having its radial and angular parts as $u_\ell(r_1)$ and $Y_m^\ell(\hat{\mathbf{r}}_1)$, respectively, which are associated with the relative motion of b and c . Integrals over the internal coordinates ξ give

$$\int d\xi \Phi_b^*(\xi_b) \Phi_c^*(\xi_c) \Phi_a(\xi_a, \mathbf{r}_1) = \sum_{\ell m j_c \mu_c} \langle \ell m j_c \mu_c | j \mu \rangle \langle j_b \mu_b j \mu | j_a \mu_a \rangle i^\ell u_\ell(r_1) Y_m^\ell(\hat{\mathbf{r}}_1). \quad (51)$$

In Eq. (51), ℓ is the orbital angular momentum for the relative motion between

b and c , j_a is the spin of a . Using this equation the T -matrix can be written as

$$T = \sum_{\ell m j \mu} \langle \ell m j_c \mu_c | j \mu \rangle \langle j_b \mu_b j \mu | j_a \mu_a \rangle i^\ell \hat{\ell} \beta_{\ell m}(\mathbf{k}_b, \mathbf{k}_c; \mathbf{k}_a), \quad (52)$$

where

$$\begin{aligned} \hat{\ell} \beta_{\ell m}(\mathbf{k}_b, \mathbf{k}_c; \mathbf{k}_a) = & \int \int d\mathbf{r}_1 d\mathbf{r}_i \chi_b^{(-)*}(\mathbf{k}_b, \mathbf{r}) e^{-i\mathbf{k}_c \cdot \mathbf{r}_c} V_{bc}(\mathbf{r}_1) \\ & \times \phi_a^{\ell m}(\mathbf{r}_1) \chi_a^{(+)}(\mathbf{k}_a, \mathbf{r}_i), \end{aligned} \quad (53)$$

with $\beta_{\ell m}$ being the reduced T - matrix and $\hat{\ell} = \sqrt{2\ell + 1}$. We have written $\phi_a^{\ell m}(\mathbf{r}_1) = u_\ell(r_1) Y_m^\ell(\hat{\mathbf{r}}_1)$.

It may be noted that the reduced amplitude $\beta_{\ell m}$ involves a six dimensional integral which makes its evaluation quite complicated. The problem gets further acute due to the fact that the integrand involves three scattering waves which have oscillatory behaviour asymptotically. Therefore, several approximate methods have been used in the literature to avoid the evaluation of six dimensional integrals. In the zero range approximation (ZRA) [41] one assumes

$$V_{bc}(\mathbf{r}_1) \phi_a^{\ell m}(\mathbf{r}_1) = D_0 \delta(\mathbf{r}_1), \quad (54)$$

where D_0 is the usual zero range constant. This approximation reduces the six dimensional integral in Eq. (53) to a three-dimensional one. The corresponding amplitude is written as

$$\beta_{00}^{ZR} = D_0 \langle \chi_b^{(-)}(\mathbf{k}_b, \mathbf{r}_i) e^{i\delta \mathbf{k}_c \cdot \mathbf{r}_i} | \chi_a^{(+)}(\mathbf{k}_a, \mathbf{r}_i) \rangle. \quad (55)$$

In Eq. (55), the details of the projectile structure enter in the reaction amplitude only as a multiplicative constant D_0 . However, ZRA necessarily restricts the relative motion between b and c in the projectile a to s - state only. Even for such cases, this approximation may not be satisfied for heavier projectiles and at higher beam energies [74].

Baur and Trautmann (BT) [75] have proposed an alternative approximation in which the projectile c.m. coordinate in the corresponding distorted wave in Eq. (53) is replaced by that of the core-target system, i.e. $\mathbf{r}_i \approx \mathbf{r}$. With this approximation the amplitude $\beta_{\ell m}$ splits into two factors each involving a three dimensional integral

$$\hat{\ell} \beta_{\ell m}^{BT} = \langle e^{i\mathbf{k}_c \cdot \mathbf{r}_1} | V_{bc} | \phi_a^{\ell m}(\mathbf{r}_1) \rangle \langle \chi_b^{(-)}(\mathbf{k}_b, \mathbf{r}) e^{i\delta \mathbf{k}_c \cdot \mathbf{r}} | \chi_a^{(+)}(\mathbf{k}_a, \mathbf{r}) \rangle. \quad (56)$$

The first term depends on the structure of the projectile through its ground state wave function $\phi_a^{\ell m}(\mathbf{r}_1)$. The second term involves the dynamics of the reaction, which can be expressed analytically in terms of the bremsstrahlung integral [87]. This amplitude (which will be referred to as the BT amplitude), used originally to study the deuteron breakup at sub-Coulomb energies [75], was applied to calculations of the Coulomb breakup of halo nuclei in Ref. [76]. This approximation, which allows the application of the theory to non- s - wave

projectiles, may seem to be justified if the c.m of the $b - c$ system is shifted towards b (which is indeed the case if $m_b \gg m_c$). However, the neglected piece of \mathbf{r}_i ($\alpha\mathbf{r}_1$) occurs in association with the wave vector \mathbf{k}_a , whose magnitude could be quite large for the reactions at higher beam energies. Therefore, contributions coming to the amplitude from the neglected part of \mathbf{r}_i may still be substantial.

An approximate way of taking into account the finite range effects in the post form DWBA theory is provided by the local momentum approximation [74, 72]. The attractive feature of this approximation is that it leads to the factorization of the amplitude $\beta_{\ell m}$ similar to that obtained in the BT case. We use this approximation to write the Coulomb distorted wave of particle b in the final channel as

$$\chi_b^{(-)}(\mathbf{k}_b, \mathbf{r}) = e^{-i\alpha\mathbf{K}\cdot\mathbf{r}_1}\chi_b^{(-)}(\mathbf{k}_b, \mathbf{r}_i). \quad (57)$$

Eq. (57) represents an exact Taylor series expansion about \mathbf{r}_i if $\mathbf{K}(= -i\nabla_{\mathbf{r}_i})$ is treated exactly. However, this is not done in the LMA scheme. Instead, the magnitude of the local momentum is taken to be

$$K(R) = \sqrt{\frac{2m}{\hbar^2}[E - V(R)]}, \quad (58)$$

where m is the reduced mass of the $b - t$ system, E is the energy of particle b relative to the target in the c.m. system and $V(R)$ is the Coulomb potential between b and the target at a distance R . Thus, the local momentum \mathbf{K} is evaluated at some distance R , and its magnitude is held fixed for all the values of \mathbf{r} . As shown in appendix of Ref. [77], the magnitude of \mathbf{K} remains constant for $\mathbf{r} > 10$ fm. Due to the peripheral nature of breakup reactions, this region contributes maximum to the cross section. Therefore, we have taken a constant magnitude for \mathbf{K} evaluated at $R = 10$ fm for all the values of r . As is discussed in [77, 64] the results of our calculations are almost independent of the choice of the direction of the local momentum. Therefore, we have taken the directions of \mathbf{K} and \mathbf{k}_b to be the same in all the calculations. Detailed discussion on the validity of the local momentum approximation is presented in Refs. [77, 64]. It may be noted that in the calculations presented in Ref. [78], the LMA was applied to the Coulomb distorted wave of the projectile channel which could imply a deviation from the distorted wave approximation.

Substituting Eq. (57) into Eq. (53) we get the following factorized form of the reduced amplitude

$$\begin{aligned} \hat{\ell}\beta_{\ell m}^{FRDWBA} &= \langle e^{i(\gamma\mathbf{k}_c - \alpha\mathbf{K})\cdot\mathbf{r}_1} | V_{bc} | \phi_a^{\ell m}(\mathbf{r}_1) \rangle \\ &\times \langle \chi_b^{(-)}(\mathbf{k}_b, \mathbf{r}_i) e^{i\delta\mathbf{k}_c\cdot\mathbf{r}_i} | \chi_a^{(+)}(\mathbf{k}_a, \mathbf{r}_i) \rangle. \end{aligned} \quad (59)$$

Eq. (59) (which will be referred to as the FRDWBA amplitude in the following) looks like Eq. (56) of the BT theory but with the very important difference that the form factor is now evaluated at the momentum transfer $(\gamma\mathbf{k}_c - \alpha\mathbf{K})$, and not at the valence particle momentum \mathbf{k}_c . The two momenta could be quite different for cases of interest in this work. The second term, involving the dynamics of

the reaction, is the same in both the cases. Therefore, the breakup amplitude obtained in BT approximation differs from that of FRDWBA by a factor

$$F_r = \frac{\beta_{\ell m}^{BT}}{\beta_{\ell m}^{FRDWBA}} = \frac{\langle e^{i\mathbf{k}_c \cdot \mathbf{r}_1} | V_{bc} | \phi_a^{\ell m}(\mathbf{r}_1) \rangle}{\langle e^{i(\beta\mathbf{k}_c - \alpha\mathbf{K}) \cdot \mathbf{r}_1} | V_{bc} | \phi_a^{\ell m}(\mathbf{r}_1) \rangle} \quad (60)$$

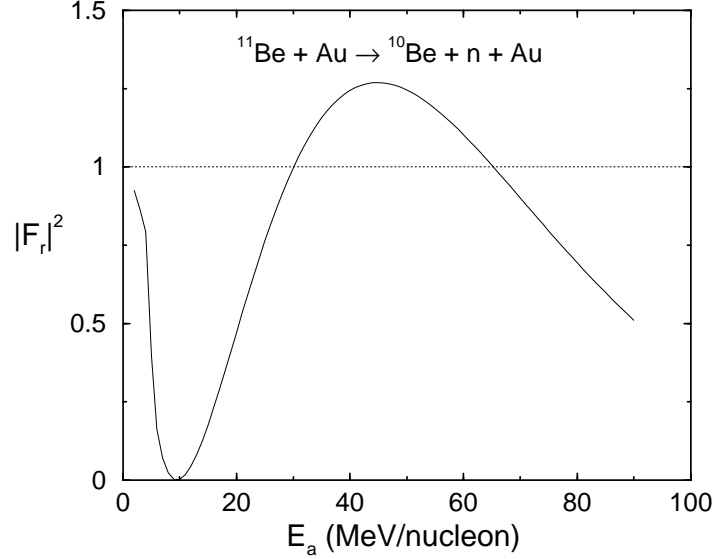


Figure 4: Modulus square of the ratio F_r defined by Eq. (60) as a function of the beam energy for the breakup of ^{11}Be on a gold target at the beam energy of 44 MeV/nucleon corresponding to forward emission angles of the breakup fragments as discussed in the text.

In Fig. 4, we have shown the beam energy dependence of $|F_r|^2$ for the breakup of ^{11}Be on a gold target at the beam energy of 44 MeV/nucleon for a set of forward angles of the outgoing fragments ($\theta_b = 1^\circ$, $\theta_c = 1^\circ$ and $\phi_c = 1^\circ$). In this calculation, the ground state wave function of ^{11}Be has been obtained by considering a configurations in which a s -wave valence neutron is coupled to 0^+ ^{10}Be core [$^{10}\text{Be}(0^+) \otimes 1s_{1/2}\nu$] with the one-neutron separation energy ($S_{n-^{10}\text{Be}}$) of 504 keV and a spectroscopic factor (SF) of 0.74 [79, 80, 81]. The single particle wave function has been obtained by assuming the valence neutron- ^{10}Be interaction to be of Woods-Saxon type whose depth is adjusted to reproduce the corresponding binding energy with fixed values of the radius and diffuseness parameters (taken to be 1.15 fm and 0.5 fm, respectively)(see [77] for more details). In this figure, we see that $|F_r|^2$ is close to unity only at the sub-Coulomb beam energies (of course at higher beam energies it crosses twice the line representing the value 1). Therefore, the BT and FRDWBA calculations

are expected to produce similar results at very low incident energies. Depending upon the beam energy, the BT results can be larger or smaller than those of the FRDWBA.

Recently, a theory of the Coulomb breakup has been developed within an adiabatic (AD) model [82, 83], where one assumes that the excitation of the projectile is such that the relative energy (ϵ_{bc}) of the $b - c$ system is much smaller than the total incident energy, which allows ϵ_{bc} to be replaced by the constant separation energy of the fragments in the projectile ground state. It was shown in [83] that under these conditions the wave function $\Psi_a^{(+)}(\xi_a, \mathbf{r}_1, \mathbf{r}_i)$ has an exact solution as given below

$$\Psi_a^{(+),AD}(\xi_a, \mathbf{r}_1, \mathbf{r}_i) = \Phi_a(\xi_a, \mathbf{r}_1)e^{i\alpha\mathbf{k}_a \cdot \mathbf{r}_1}\chi_a^{(+)}(\mathbf{k}_a, \mathbf{r}). \quad (61)$$

Substituting $\Psi_a^{(+),AD}$ for $\Psi_a^{(+)}$ in Eq. (50) leads to the reduced amplitude:

$$\hat{\ell}\beta_{\ell m}^{AD} = \langle e^{i(\mathbf{k}_c - \alpha\mathbf{k}_a) \cdot \mathbf{r}_1} | V_{bc} | \phi_a^{\ell m}(\mathbf{r}_1) \rangle \langle \chi_b^{(-)}(\mathbf{k}_b, \mathbf{r}) | e^{i\delta\mathbf{k}_c \cdot \mathbf{r}} | \chi_a^{(+)}(\mathbf{k}_a, \mathbf{r}) \rangle. \quad (62)$$

This amplitude differs from those of BT as well as FRDWBA only in the form factor part (first term), which is evaluated here at the momentum transfer ($\mathbf{k}_c - \alpha\mathbf{k}_a$). Eq. (62) can also be obtained in the DWBA model by making a local momentum approximation to the Coulomb distorted wave in the initial channel of the reaction, and by evaluating the local momentum at $R = \infty$ with its direction being the same as that of the projectile [78]. The adiabatic model does not make the weak coupling approximation of the DWBA. However, it necessarily requires one of the fragments (in this case c) to be chargeless. In contrast, the FRDWBA can be applied to cases where both the fragments b and c are charged (see, e.g., Ref. [74]). While the effect of nuclear breakup in the adiabatic model description of the elastic scattering of the loosely bound projectile has been calculated in Refs. [83, 84, 85], the nuclear part of the amplitude for breakup reactions is yet to be calculated within this model. However, the calculations of the nuclear breakup cross section has been done within the FRDWBA theory [64].

The triple differential cross section of the reaction is given by

$$\frac{d^3\sigma}{dE_b d\Omega_b d\Omega_c} = \frac{2\pi}{\hbar v_a} \rho(E_b, \Omega_b, \Omega_c) \sum_{\ell m} |\beta_{\ell m}|^2, \quad (63)$$

where $\rho(E_b, \Omega_b, \Omega_c)$ is the appropriate [86] three-body phase space factor, given by

$$\rho(E_b, \Omega_b, \Omega_c) = \frac{\hbar^{-6} m_b m_c m_t p_b p_c}{m_t + m_c - m_c \frac{\mathbf{k}_c \cdot (\mathbf{k}_a - \mathbf{k}_b)}{k_c^2}}, \quad (64)$$

with \mathbf{k}_a , \mathbf{k}_b and \mathbf{k}_c being evaluated in the appropriate frame of reference. v_a is the relative velocity of the projectile in the initial channel. In Eq. (64), the linear momenta, p , are related to wave numbers k by $p = \hbar k$.

Substituting the following expressions for the Coulomb distorted waves

$$\chi_b^{(-)*}(\mathbf{k}_b, \mathbf{r}_i) = e^{-\pi\eta_b/2}\Gamma(1+i\eta_b)e^{-i\mathbf{k}_b\cdot\mathbf{r}_i}{}_1F_1(-i\eta_b, 1, i(k_b r_i + \mathbf{k}_b\cdot\mathbf{r}_i)), \quad (65)$$

$$\chi_a^{(+)}(\mathbf{k}_a, \mathbf{r}_i) = e^{-\pi\eta_a/2}\Gamma(1+i\eta_a)e^{i\mathbf{k}_a\cdot\mathbf{r}_i}{}_1F_1(-i\eta_a, 1, i(k_a r_i - \mathbf{k}_a\cdot\mathbf{r}_i)) \quad (66)$$

in Eq. (59), one gets for the triple differential cross section

$$\frac{d^3\sigma}{dE_b d\Omega_b d\Omega_c} = \frac{2\pi}{\hbar v_a} \rho(E_b, \Omega_b, \Omega_c) \frac{4\pi^2 \eta_a \eta_b}{(e^{2\pi\eta_b} - 1)(e^{2\pi\eta_a} - 1)} |I|^2 4\pi \sum_{\ell} |Z_{\ell}|^2. \quad (67)$$

In Eqs. (65 – 67), η 's are the Coulomb parameters for the concerned particles. In Eq. (67), I is the bremsstrahlung integral [87] which can be evaluated in a closed form:

$$I = -i \left[B(0) \left(\frac{dD}{dx} \right)_{x=0} (-\eta_a \eta_b) {}_2F_1(1 - i\eta_a, 1 - i\eta_b; 2; D(0)) \right. \\ \left. + \left(\frac{dB}{dx} \right)_{x=0} {}_2F_1(-i\eta_a, -i\eta_b; 1; D(0)) \right], \quad (68)$$

where

$$B(x) = \frac{4\pi}{k^{2(i\eta_a + i\eta_b + 1)}} \left[(k^2 - 2\mathbf{k}\cdot\mathbf{k}_a - 2xk_a)^{i\eta_a} (k^2 - 2\mathbf{k}\cdot\mathbf{k}_b - 2xk_b)^{i\eta_b} \right], \quad (69)$$

$$D(x) = \frac{2k^2(k_a k_b + \mathbf{k}_a\cdot\mathbf{k}_b) - 4(\mathbf{k}\cdot\mathbf{k}_a + xk_a)(\mathbf{k}\cdot\mathbf{k}_b + xk_b)}{(k^2 - 2\mathbf{k}\cdot\mathbf{k}_a - 2xk_a)(k^2 - 2\mathbf{k}\cdot\mathbf{k}_b - 2xk_b)} \quad (70)$$

with $\mathbf{k} = \mathbf{k}_a - \mathbf{k}_b - \delta\mathbf{k}_c$. Z_{ℓ} contains the projectile structure information and is given by

$$Z_{\ell} = \int dr_1 r_1^2 j_{\ell}(k_1 r_1) V_{bc}(\mathbf{r}_1) u_{\ell}(r_1), \quad (71)$$

with $k_1 = |\gamma\mathbf{k}_c - \alpha\mathbf{K}|$.

Let us now discuss some numerical applications of the theory of the pure Coulomb breakup reactions as presented above. We investigate the breakup of neutron rich nuclei ${}^{11}\text{Be}$ and ${}^{15,17,19}\text{C}$ at beam energies below 100 MeV/nucleon. Apart from the distance at which the local momentum is calculated (which is taken to be 10 fm) and its direction (described earlier), the only other input to our calculations is the radial part of the projectile ground state wave function. As discussed above, we have assumed a Woods-Saxon potential to describe the valence neutron-core relative motion whose depth is searched, for a given configuration, to reproduce the corresponding binding energy. In the calculations presented here we have mostly considered a s -wave configuration (as described above) for the ${}^{11}\text{Be}$ ground state. However, in some cases we have also considered a d -wave configuration for this nucleus in which a d -wave valence neutron is coupled to $2^+ {}^{10}\text{Be}$ core [${}^{10}\text{Be}(2^+) \otimes 0d_{5/2}\nu$] with the one-neutron separation

energy (S_{n-10Be}) of 3.872 MeV [77]. The configurations for the C isotopes used in our calculations are described at the appropriate places below.

In Fig. 5, we present a comparison of our calculation with the data (taken from [70]) for the neutron energy distribution of the double differential cross section ($d^2\sigma/dE_n d\Omega_n$) at the neutron angles of 1° and 3.4° , in the breakup of ^{11}Be on a gold target at the beam energy of 44 MeV/nucleon. Calculations performed within both FRDWBA and AD model of pure Coulomb breakup are shown in this figure. The s -wave configuration has been used for the ^{11}Be

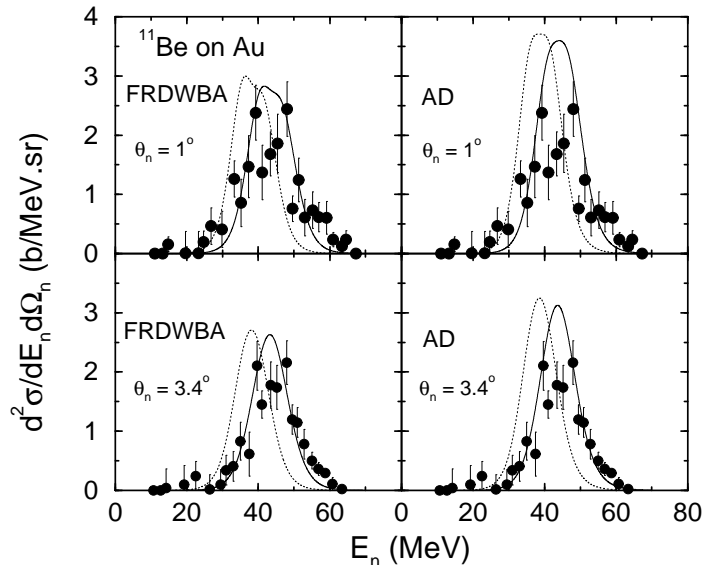


Figure 5: Neutron energy distributions for the breakup of ^{11}Be on Au at beam energies of 37 MeV/nucleon (dotted lines) and 44 MeV/nucleon (solid lines), calculated using configuration (a) with single particle wave functions within the FRDWBA and the AD models. The top half of the figure is for $\theta_n = 1^\circ$, while the bottom half is for $\theta_n = 3.4^\circ$. The experimental data are taken from [70].

ground state in both the cases. The beam energy in this experiment [70] varies between 36.9 – 44.1 MeV/nucleon. To take into account this spread, we have performed calculations at both its upper (44 MeV/nucleon) (solid line) and lower ends (37 MeV/nucleon) (dotted line). Even though these data have large statistical errors, the calculations performed at 44 MeV/nucleon are in better agreement with the experimental values. It should also be noted that the AD model calculations over-predict the experimental cross sections in the peak region.

The measured neutron angular distribution in the exclusive $^{11}\text{Be} + A \rightarrow ^{10}\text{Be} + n + A$ reaction on heavy targets below the grazing angle is very narrow and is shown to be [78, 88] dominated by the Coulomb breakup process. This

reflects the narrow width of the transverse momentum distribution of the valence neutron in the ground state of ^{11}Be , which is consistent with the presence of a neutron halo structure in ^{11}Be . In Fig. 6, we compare the calculated and measured exclusive neutron angular distribution $d\sigma/d\Omega_n$ as a function of the neutron angle θ_n for the above reaction on Au, Ti and Be targets at the beam energy of 41 MeV/nucleon. The ^{11}Be ground state wave function is the same as described above. We note that for Au and Ti targets pure coulomb breakup calculations are able to describe the data at forward angles (for neutron angles below 25° and 15° , respectively in the two case). On the other hand, for the ^9Be target pure breakup calculations are much below the data everywhere. This gives a clear indication of the importance of nuclear breakup effects at the backward angles for the medium mass and heavy targets and everywhere for the light target.

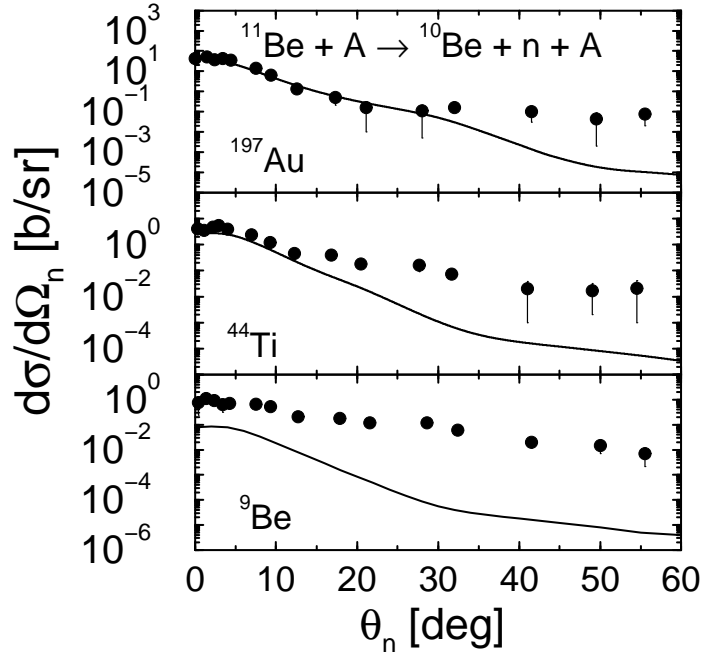


Figure 6: The calculated neutron angular distributions for the breakup of ^{11}Be on a Au, Ti and Be targets at 41 MeV/nucleon beam energy. The data are taken from [70].

Pure Coulomb contribution to the relative energy spectrum in the breakup of ^{11}Be on a Pb target at 72 MeV/nucleon is shown in Fig. 7. The top half shows the results obtained with FRDWBA (solid line), AD model (dotted line) and the BT approximation (dashed line) using the s -wave configuration for the ^{11}Be ground state. In the bottom half, we show additionally the results obtained with the ^{11}Be wave function calculated within a dynamical core polarization (DCP) model [89] (dotted line) and that obtained with the d -wave

configuration as described above. We see that, while both the FRDWBA and the AD model calculations reproduce the peak value of the data [90] well, the FRDWBA calculations done with the DCP wave function overestimate it. On the other hand, none of the calculations is able to explain the data at higher relative energies. This can be attributed to the fact that nuclear breakup effects, which can contribute substantially [91] at higher relative energies (for $E_{rel} > 0.6$ MeV), are not included in these calculations. Of course, authors of Ref. [90] claim that their data have been corrected for these contributions. However, the procedure adopted by them for this purpose is inadequate. They obtained the nuclear breakup contribution on the Pb target, by scaling the cross sections measured on a carbon target. This scaling procedure is unlikely to be accurate for reactions induced by halo nuclei due to the presence of a long tail in their ground state.

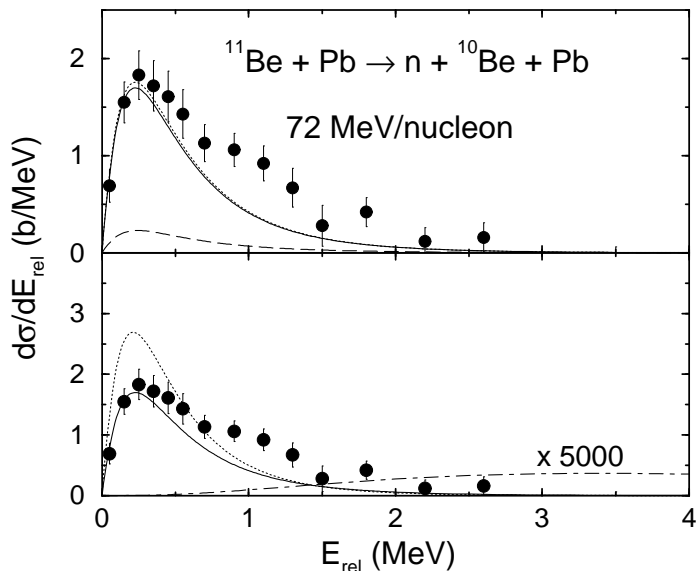


Figure 7: Relative energy spectra for the Coulomb breakup of ^{11}Be on a Pb target at 72 MeV/nucleon beam energy. The top half of the figure shows the spectra obtained with a single particle wave function, using the FRDWBA (solid line), the AD model (dotted line) and the BT approximation (dashed line). The bottom half shows the results of FRDWBA calculations using single particle (solid line) and DCP (dotted line) wave functions. The dot-dashed line shows the d – state FRDWBA calculation using a single particle wave function, after being multiplied by a factor of 5000. The data are taken from [90].

In a full quantum mechanical theory, both Coulomb and nuclear breakup contributions should be calculated on the same footing and corresponding amplitudes should be added coherently. This is discussed in the next section.

Calculations done using the BT theory (dashed line in the upper part of Fig. 7) underestimates the data considerably. This difference between the FRDWBA and the BT results can again be traced to the behaviour of $|F_r|^2$ in Fig. 4, which is smaller than unity at the beam energy of 72 MeV/nucleon of this reaction. The FRDWBA result using the d -state configuration with single particle wave function (dot-dashed line in the lower half of Fig. 7, shown after multiplying the actual numbers by 5000) also grossly underestimates the data.

The neutron halo structure is reflected in the narrow width of the parallel momentum distribution (PMD) of the charged breakup fragments emitted in breakup reactions induced by the halo nuclei. This is because the PMD is least affected by the reaction mechanism [92, 93, 94, 95, 96] and therefore, a narrow PMD can be related to a long tail in the matter distribution in the coordinate space via Heisenberg's uncertainty principle.

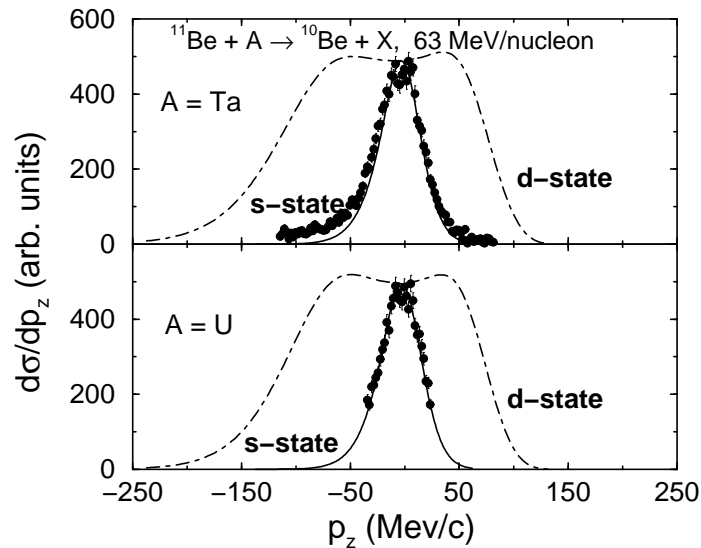


Figure 8: Parallel momentum distributions of ^{10}Be in the breakup of ^{11}Be on Ta (top half) and U (bottom half) at the beam energy of 63 MeV/nucleon, in the rest frame of the projectile, with s -wave (solid line) and d -wave (dot-dashed line) configurations for the ^{11}Be ground state. Both calculations are done in FRDWBA and are normalized to the data peaks. The data are taken from [93].

In Fig. 8, we present the PMD of the ^{10}Be fragment emitted in the breakup of ^{11}Be on U and Ta targets at 63 MeV/nucleon beam energy. Calculations performed within the FRDWBA and the AD models using both the s -wave and d -wave configurations are presented in this figure. The calculated cross sections are normalized to match the peak of the data points (which are given in arbitrary units) [93], the normalization constant being the same for both cases. With the s -wave configuration the full width at half maximum (FWHM) for the U and Ta targets are 44 MeV/c and 43 MeV/c, respectively in both the

FRDWBA and the AD cases. These agree well with the averaged experimental value of 43.6 ± 1.1 MeV/c [93] and also with those calculated in [78]. The very narrow widths of the parallel momentum distributions signal the presence of a neutron halo structure in ^{11}Be . It may be noted that the PMD calculated with a pure d – wave configuration is too wide in width and grossly overestimates the experimental FWHM.

In Fig. 9, we present the PMD (calculated within the FRDWBA formalism) of the ^{18}C fragment in the breakup of ^{19}C on a Ta target at the beam energy of 88 MeV/nucleon. We have normalized the peaks of the calculated PMDs to

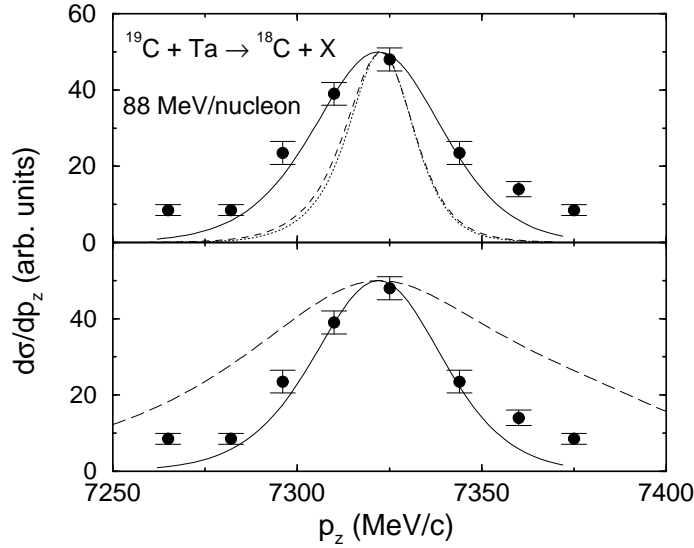


Figure 9: FRDWBA results for the parallel momentum distribution of ^{18}C in the breakup of ^{19}C on Ta target at the beam energy of 88 MeV/nucleon. The top half shows the results obtained with the configuration $[^{18}\text{C}(0^+) \otimes 1s_{1/2}\nu]$ and single particle wave function for the ground state of ^{19}C with one-neutron separation energies of 530 keV (solid line), 160 keV (dashed line). The dotted line shows the result obtained with a DCP wave function with a one-neutron separation energy of 160 keV. The bottom half shows the result obtained with the configurations $[^{18}\text{C}(0^+) \otimes 1s_{1/2}\nu]$ (solid) and $[^{18}\text{C}(0^+) \otimes 0d_{5/2}\nu]$ (dashed), with the same value of the one-neutron separation energy (530 keV). The data have been taken from [94].

that of the data (given in arbitrary units) [94] (this also involves coinciding the position of maxima of the calculated and experimental PMDs). As can be seen from the upper part of this figure, the experimental data clearly favour $S_{n-^{18}\text{C}} = 0.53$ MeV with the s – wave n - ^{18}C relative motion in the ground state of ^{19}C (solid line). The results obtained with the s – wave configuration within the

simple potential (dashed line) and DCP (dotted line) models (with the same value of $S_{n-18C} = 0.16$ MeV) are similar to each other.

In the lower part of Fig. 9, we have shown the results obtained with the d – wave relative motion (dashed line) for this system (with $S_{n-18C} = 0.53$ MeV) and have compared it with that obtained with a s – wave relative motion (solid line) with the same value of the binding energy. As can be seen, the FWHM of the experimental PMD is grossly overestimated by the d – wave configuration. The calculated FWHM with the s – state configuration (with $S_{n-18C} = 530$ keV) is 40 MeV/c, which is in excellent agreement with the experimental value of 41 ± 3 MeV/c [94]. Thus these data favour a configuration [$^{18}\text{C}(0^+) \otimes 1s_{1/2}\nu$], with a one-neutron separation energy of 0.530 MeV for the ground state of ^{19}C . These results are in agreement with those of Ref. [97]. The narrow width of the PMD provides support to the presence of a one-neutron halo structure in ^{19}C .

We next consider the breakup of ^{15}C which has a relatively larger value for the one-neutron separation energy (1.2181 MeV) and a ground state spin-parity of $1/2^+$ [94]. We consider two configurations: a $1s_{1/2}$ neutron coupled to a $^{14}\text{C}(0^+)$ core and a $0d_{5/2}$ neutron coupled to a $^{14}\text{C}(0^+)$ core. One could have also considered a $^{14}\text{C}(2^+)$ core and $0d_{5/2}$ neutron coupling to get a $1/2^+$ ground state for ^{15}C , but it would raise the one-neutron separation energy to about 7.01 MeV, which is highly unfavourable for the formation of a halo. We, therefore, do not consider this configuration in our study.

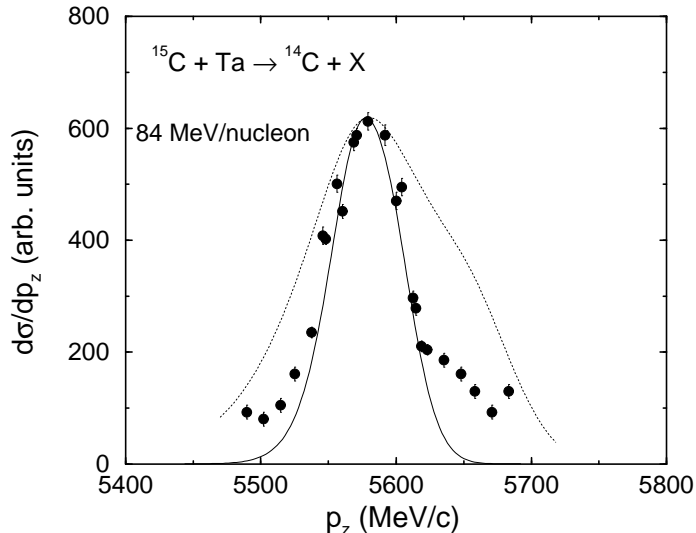


Figure 10: Parallel momentum distributions of ^{14}C in the breakup of ^{15}C on Ta at 84 MeV/nucleon. The solid line and dotted lines show the results obtained with the configurations [$^{14}\text{C}(0^+) \otimes 1s_{1/2}\nu$] and [$^{14}\text{C}(0^+) \otimes 0d_{5/2}\nu$], respectively for the ground state of the projectile. The data have been taken from [94].

Table 1: FWHMs from the parallel momentum distribution of ^{16}C for different ground state configurations of ^{17}C and one-neutron separation energies (ϵ) in the breakup of ^{17}C on Ta at 84 MeV/nucleon beam energy.

Projectile configuration	ϵ (MeV)	$FWHM$ (MeV/c)
$^{16}\text{C} (0^+) \otimes 1s_{1/2}\nu$	0.729	51
$^{16}\text{C} (0^+) \otimes 0d_{5/2}\nu$	0.729	114
$^{16}\text{C} (2^+) \otimes 1s_{1/2}\nu$	2.5	82
$^{16}\text{C} (2^+) \otimes 0d_{5/2}\nu$	2.5	185

In Fig. 10, we present the results of our calculations for the PMD of the ^{14}C fragment in the breakup of ^{15}C on a Ta target at the beam energy of 84 MeV/nucleon. The experimental data are taken from [94]. The s – state configuration for the ground state of ^{15}C gives a FWHM of 62 MeV/c, while with the d – state configuration it comes out to be 140 MeV/c. Therefore, the experimental value for the FWHM (67 ± 1 MeV/c) [94] favours the former configuration. Thus, our results provide support to the existence of a halo structure in ^{15}C . This nucleus provides an example of the one-neutron halo system with the largest one-neutron separation energy, known so far.

^{17}C has a lower one-neutron separation energy (729 keV) as compared to that of ^{15}C . It would be interesting to see if it also has a halo structure, which seems probable if one considers only the binding energies. The quoted ground state spin-parities for this nucleus are $1/2^+$, $3/2^+$ and $5/2^+$ [98]. RMF calculations [99] predict it to have a value of $3/2^+$. We consider four possible ground state configurations for this nucleus and calculate the parallel momentum distributions of the ^{16}C fragment in the breakup of ^{17}C on a Ta target at 84 MeV/nucleon beam energy within our FRDWBA formalism. The FWHMs of the PMD obtained with different configurations are listed in Table 1.

It is evident from this table that the s – state configurations predict a narrow width for the PMD, providing support to the existence of a halo structure in this nucleus. The experimental data [94] for the breakup of ^{17}C on a light target (Be) at 84 MeV/nucleon give a FWHM of 145 ± 5 MeV/c. Since the width of the PMD is mostly unaffected by the reaction mechanism [78], it is quite likely that the experimental FWHM will be the same also for the breakup of this nucleus on a heavier target. Therefore, the results shown in Table 1 seem to provide support to a d – wave configuration for the ground state of ^{17}C [100]. Hence, the existence of a one-neutron halo structure is quite improbable in ^{17}C (see also Refs. [101, 102]).

In summary, from our pure Coulomb breakup studies we can say that the nuclei ^{11}Be , ^{19}C and ^{15}C have a one-neutron halo structure in their ground states.

However, for ^{17}C such a structure appears to be less likely. The calculated cross sections are selective about the ground state wave function of the projectile. At the same time there is a clear indication of the fact that only pure Coulomb or pure nuclear breakup calculations may not be sufficient to describe the details of the halo breakup data. Consideration of both modes of breakup as well as of their interference terms is necessary to describe the data properly.

3.2 Full breakup amplitude

The full breakup amplitude that includes consistently both Coulomb and nuclear interactions between the projectile fragments and the target nucleus to all orders has been developed in Refs. [63, 64]. We perform a Taylor series expansion of the distorted waves of particles b and c about \mathbf{r}_i and write

$$\chi_b^{(-)}(\mathbf{k}_b, \mathbf{r}) = e^{-i\alpha\mathbf{K}_b \cdot \mathbf{r}_1} \chi_b^{(-)}(\mathbf{k}_b, \mathbf{r}_i), \quad (72)$$

$$\chi_c^{(-)}(\mathbf{k}_c, \mathbf{r}_c) = e^{i\gamma\mathbf{K}_c \cdot \mathbf{r}_1} \chi_c^{(-)}(\mathbf{k}_c, \delta\mathbf{r}_i). \quad (73)$$

Employing the LMA [74, 72], the magnitudes of momenta \mathbf{K}_j are taken as

$$K_j(R) = \sqrt{(2m_j/\hbar^2)[E_j - V_j(R)]}, \quad (74)$$

where m_j ($j = b, c$) is the reduced mass of the $j - t$ system, E_j is the energy of particle j relative to the target in the center of mass (c.m.) system, and $V_j(R)$ is the potential between j and t at a distance R . Substituting Eqs. (72) and (73) in Eq. (50), and introducing the partial wave expansion of the distorted waves and carrying out the angular momentum algebra, one gets

$$\begin{aligned} \hat{\ell}\beta_{\ell m} &= \frac{(4\pi)^3}{k_a k_b k_c \delta} i^{-\ell} Y_{m\ell}^{\ell}(\hat{\mathbf{Q}}) Z_{\ell}(Q) \sum_{L_a L_b L_c} (i)^{L_a - L_b - L_c} \hat{L}_b \hat{L}_c \\ &\times \mathcal{Y}_{L_c}^{L_b}(\hat{k}_b, \hat{k}_c) \langle L_b 0 L_c 0 | L_a 0 \rangle \mathcal{R}_{L_b, L_c, L_a}(k_a, k_b, k_a), \end{aligned} \quad (75)$$

where

$$\mathcal{Y}_{L_c}^{L_b}(\hat{k}_b, \hat{k}_c) = \sum_M (-)^M \langle L_b M L_c - M | L_a 0 \rangle Y_M^{L_b}(\hat{k}_b) Y_M^{L_c*}(\hat{k}_c), \quad (76)$$

$$Z_{\ell}(Q) = \int_0^{\infty} r_1^2 dr_1 j_{\ell}(Qr_1) u_{\ell}(r_1) V_{bc}(r_1), \quad (77)$$

$$\mathcal{R}_{L_b, L_c, L_a} = \int_0^{\infty} \frac{dr_i}{r_i} f_{L_a}(k_a, r_i) f_{L_b}(k_b, r_i) f_{L_c}(k_c, \delta r_i). \quad (78)$$

In Eq. (75), Q is the magnitude of the vector $\mathbf{Q} = \gamma\mathbf{K}_c - \alpha\mathbf{K}_b$. Functions f appearing in the radial integral $\mathcal{R}_{L_b, L_c, L_a}(k_a, k_b, k_a)$ are the radial parts of the distorted wave functions χ 's. These are obtained by solving the Schrödinger equation with appropriate optical potential which include both Coulomb and nuclear terms. The slowly converging radial integral $\mathcal{R}_{L_b, L_c, L_a}$ are effectively handled by using the complex plane method [103, 104].

This theory can be used to calculate breakup of both neutron and proton halo nuclei. Generally, the maximum value of the partial waves L_a, L_b, L_c must be very large in order to ensure the convergence of the partial wave summations in Eq. (75). However, for the case of one-neutron halo nuclei, one can make use of the following method to include summations over infinite number of partial waves. We write $\beta_{\ell m}$ as

$$\beta_{\ell m} = \sum_{L_i=0}^{L_i^{max}} \hat{\beta}_{\ell m}(L_i) + \sum_{L_i=L_i^{max}}^{\infty} \hat{\beta}_{\ell m}(L_i), \quad (79)$$

where $\hat{\beta}$ is defined in the same way as Eq. (75) except for the summation sign and L_i corresponds to L_a, L_b , and L_c . If the value of L_i^{max} is chosen to be appropriately large, the contribution of the nuclear field to the second term of Eq. (79) can be neglected and we can write

$$\sum_{L_i=L_i^{max}}^{\infty} \hat{\beta}_{\ell m}(L_i) \approx \sum_{L_i=0}^{\infty} \hat{\beta}_{\ell m}^{Coul}(L_i) - \sum_{L_i=0}^{L_i^{max}} \hat{\beta}_{\ell m}^{Coul}(L_i), \quad (80)$$

where the first term on the right hand side, is the pure Coulomb breakup amplitude which for the case where one of the outgoing fragments is uncharged, can be expressed analytically in terms of the bremsstrahlung integral (see, e.g., Ref. [77]). Therefore, only two terms, with reasonable upper limits, are required to be evaluated by the partial wave expansion in Eq. (79).

In the numerical applications for the breakup of ^{11}Be , the structure function Z_ℓ has been calculated with the s -wave configuration for the ^{11}Be ground state. The neutron-target optical potentials were extracted from the global set of Bechetti-Greenlees (see, e.g, [105]), while those for the ^{10}Be -target system were taken from ([105, 106]). Following [62], we have used the sum of these two potentials for the ^{11}Be -target channel (see, [64] for more details). We found that values of L_i^{max} of 500 for Au, Ta, U, Pb and Ti targets and 150 for Be and C targets provided very good convergence of the corresponding partial wave expansion series. The local momentum wave vectors are evaluated at a distance, $R = 10$ fm, in all the cases with their directions being the same as that of asymptotic momenta.

In Fig. 11, we show our results for the neutron angular distributions ($d\sigma/d\Omega_n$) for the breakup of ^{11}Be on Au, Ti and Be targets at 41 MeV/nucleon. The neutron energy has been integrated from 26 MeV to 80 MeV, and the core scattering angle in the lab system (θ_b) has been integrated from 0° to 30° for the Au target case and from 0° to 20° for Ti and Be target cases. The dotted and dashed lines represent the pure Coulomb and nuclear contributions, respectively while their coherent sums are shown by the solid lines. The plus signs and the inverted solid triangles represent the magnitudes of the positive and negative interference terms, respectively. Our calculations are in good agreement with the experimental data [70] (shown by solid circles) for all the three targets.

For the Be target, $d\sigma/d\Omega_n$ is governed solely by the nuclear breakup effects at all the angles. The pure Coulomb breakup contributions are down by at least

an order of magnitude at the forward angles and by 2-3 orders of magnitude at the backward angles. The CNI terms are also small in this case.

On the other hand, for Ti and Au targets the Coulomb terms are dominant at the forward angles while the nuclear breakup effects are important at larger angles. This is to be expected for high-Z targets, as the strong Coulomb field causes the fragile halo system to breakup at large distances (and hence large impact parameters), leading to the predominance of Coulomb breakup at forward angles. The nuclear breakup assumes importance when the breakup occurs near the target nucleus, consequently leading to large scattering angles.

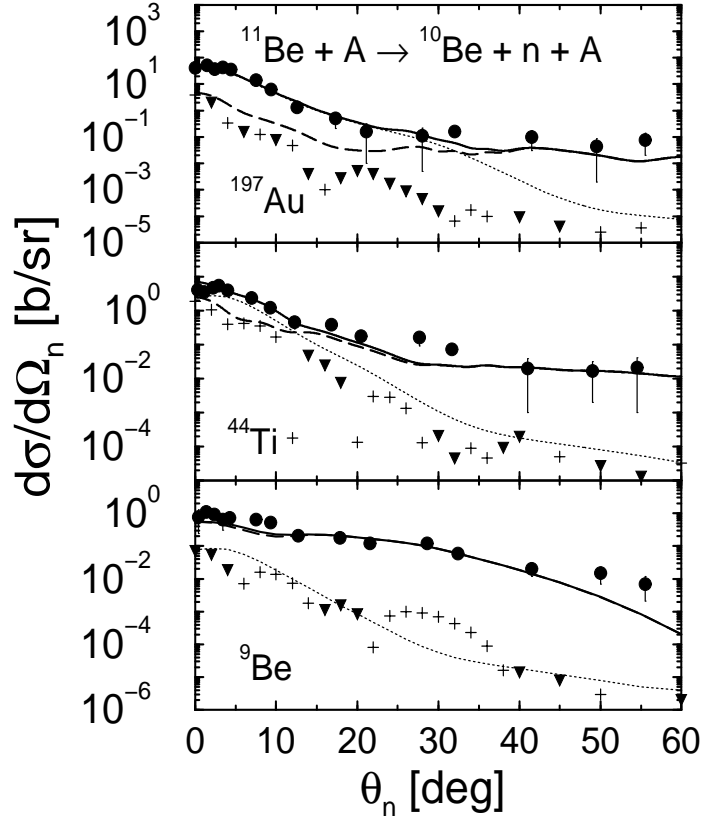


Figure 11: Neutron angular distribution for the breakup reaction $^{11}\text{Be} + A \rightarrow ^{10}\text{Be} + n + A$ at the beam energy of 41 MeV/nucleon. The dotted and dashed lines represent the pure Coulomb and nuclear contributions, respectively while their coherent sums are shown by the solid lines. The plus signs and the inverted solid triangles represent the magnitudes of the positive and negative interference terms, respectively. The data are taken from [70].

Magnitudes of the CNI terms vary with angle; for many forward angles they almost coincide with those of the nuclear breakup while at the backward angles they are closer to the pure Coulomb breakup contributions. Signs of these terms also change with the neutron angle; a feature common to all the three targets. It is clear that the interference terms are not negligible for Ti and Au targets at the forward angles. For $\theta_n \leq 10^\circ$, the magnitudes of the CNI contributions are similar to those of the pure nuclear terms, leading to a better description of the data in this region.

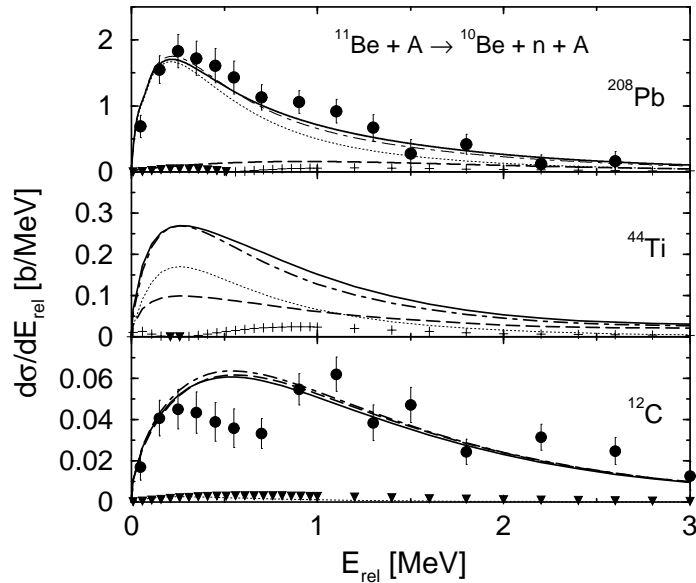


Figure 12: The differential cross section as a function of the relative energy of the fragments (neutron and ^{10}Be) in the breakup reaction of ^{11}Be on ^{208}Pb , ^{44}Ti and ^{12}C targets at 72 MeV/nucleon. The dotted and dashed lines represent the pure Coulomb and nuclear breakup contributions, respectively while their coherent and incoherent sums are shown by the solid and dot-dashed lines, respectively. The plus signs and the inverted triangles represent the magnitudes of the positive and negative interference terms, respectively. The data are taken from [90].

The relative energy spectrum of the fragments (neutron and ^{10}Be) emitted in the breakup of ^{11}Be on ^{208}Pb (top panel), ^{44}Ti (middle panel) and ^{12}C (bottom panel) targets at the beam energy of 72 MeV/nucleon is shown in Fig. 12. In these calculations the integration over the projectile c.m. angle ($\theta_{n^{10}\text{Be-Pb}}$) has been done in the range of 0° – 40° , mainly to include the effects of nuclear breakup coming from small impact parameters. The relative angle between the fragments ($\theta_{n-^{10}\text{Be}}$) has been integrated from 0° to 180° . The dotted and

dashed lines represent the pure Coulomb and nuclear breakup contributions, respectively while their coherent and incoherent sums are shown by the solid and dot-dashed lines, respectively. The plus signs and the inverted triangles represent the magnitudes of the positive and negative interference terms, respectively.

In case of breakup on a heavy target (^{208}Pb) [Fig. (12)(top panel)] the pure Coulomb contributions dominate the cross sections around the peak value, while at larger relative energies nuclear breakup gains importance. This is attributed to the different energy dependence of the two contributions [62]. The nuclear breakup occurs when the projectile and the target nuclei are close to each other. Its magnitude, which is determined mostly by the geometrical conditions, has a weak dependence on the relative energy of the outgoing fragments beyond a certain minimum value. In contrast, the Coulomb breakup contribution has a long range and it shows a strong energy dependence. The number of virtual photons increases for small excitation energies and hence the cross sections rise sharply at low excitation energies. After a certain value of this energy the cross sections decrease due to setting in of the adiabatic cut-off. The coherent sum of the Coulomb and nuclear contributions provides a good overall description of the experimental data. The nuclear and the CNI terms are necessary to explain the data at larger relative energies.

In the middle panel of Fig. (12), we show the relative energy of the fragments in the breakup of ^{11}Be on a medium mass target (^{44}Ti). At low relative energies the pure Coulomb contributions are slightly higher than the pure nuclear ones, while at higher relative energies it is the nuclear part which dominates. Apart from the very low relative energy region the CNI terms play an important role, which is clearly borne out by the difference in the coherent (solid) and incoherent (dot-dashed) sums of the pure Coulomb and pure nuclear contributions.

The relative energy spectra for the breakup on a light target (^{12}C) is shown in the bottom panel of Fig. (12). In this case we have used the same optical potential for the ^{10}Be - ^{12}C system as in the ^{10}Be - ^9Be case, which we had used earlier in calculating the neutron angular distribution in Ref. [63]. The total cross section in this case is normalized to the experimental cross section (found by integrating the area under the data points) and the same normalization constant is used for all the cross sections in this case. The breakup is clearly seen to be nuclear dominated at all relative energies, and the pure Coulomb and CNI terms have very little contributions.

The parallel momentum distributions (PMDs) of the ^{10}Be fragment in the breakup of ^{11}Be on U and Ta targets, at 63 MeV/nucleon beam energy are presented in the rest frame of the projectile, in Fig. 13. The dotted and dashed lines show the contributions of the pure Coulomb and nuclear breakups, respectively, while their coherent sums are represented by solid lines. The coherent sum is normalized to the peak of the data, which are given in arbitrary units, and the same normalization factor has been used for the pure Coulomb and pure nuclear contributions.

The above results make it clear that the Coulomb-nuclear interference terms are both energy and angle dependent. They are almost of the same magnitude

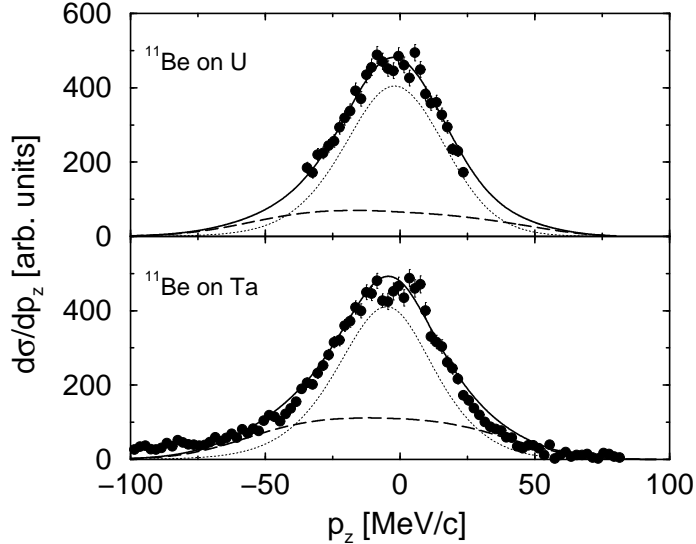


Figure 13: The parallel momentum distribution of the core in the breakup of ^{11}Be on U and Ta targets, at 63 MeV/nucleon beam energy, in the rest frame of the projectile. The dotted and dashed lines represent the pure Coulomb and nuclear breakup contributions, respectively while their coherent sums are shown by solid lines. The data are taken from [107].

as the nuclear breakup contributions in the neutron angular distributions on heavy and medium mass targets. This leads to a difference in the coherent and incoherent sums of the Coulomb and nuclear terms, more so at forward angles. In the parallel momentum distribution of the ^{10}Be fragment in the breakup reaction of ^{11}Be the region around the peak of the distribution, which gets substantial contributions from forward scattered fragments, is Coulomb dominated, while in the wings of the distribution, where contributions come from fragments scattered at large angles, the nuclear breakup contributions dominate.

The relative energy spectra of the fragments (neutron and ^{10}Be) are largely nuclear dominated for light targets. However, to explain satisfactorily the data on heavier targets one requires both the nuclear and the CNI terms particularly at higher relative energies. In case of breakup on a medium mass target, the total pure Coulomb and pure nuclear contributions were nearly equal in magnitude. Thus in many sophisticated experiments planned in the future one has to look into the role played by the CNI terms in analyzing the experimental data.

4 Postacceleration effects in the Coulomb breakup of neutron halo nuclei

As shown section 3.1, an important advantage of the post form DWBA theory of breakup reactions is that it can be solved analytically for the case of the breakup of the neutron halo nuclei with the entrance and outgoing channels involving only the Coulomb distortions [108, 76]. It constitutes an ideal “theoretical laboratory” to investigate the physics of the breakup reactions, its certain limiting cases, and its relation to other models like the semiclassical approximation. Particularly, the effect of postacceleration can be studied in a unique way within this approach.

Postacceleration refers to the situation where the core c has a larger final state energy than what one gets from sharing the kinetic energy among the fragments according to their mass ratio. This effect arises in a purely classical picture [109] of the breakup process. The nucleus $a = (c + n)$ moves up the Coulomb potential, loosing the appropriate amount of kinetic energy. At an assumed “breakup point”, this kinetic energy (minus the binding energy) is supposed to be shared among the fragments according to their mass ratio (assuming that the velocities of c and n are equal). Running down the Coulomb barrier, the charged particle c alone (and not the neutron) gains back the Coulomb energy, resulting in its postacceleration. Of course this picture is based on the purely classical interpretation of this process, and will be modified in a quantal treatment, where such a “breakup point” does not exist. Postacceleration is clearly observed in the low energy deuteron breakup, both in the theoretical calculations as well as in the corresponding experiments (see, e.g., [37, 110]). However, in the description of the Coulomb dissociation of halo nuclei at high beam energies within this theory [77, 76, 111], the postacceleration effects become negligibly small. We shall investigate this point further for the ^{11}Be and ^{19}C Coulomb dissociation experiments [90, 112]. On the other hand, in the semiclassical Coulomb excitation theory the higher order effects have been found [113] to be small, for both zero range as well as finite range wave functions of the $c + n$ system.

It was recently noticed [61] that in the limit of Coulomb parameter $\eta_a \ll 1$ (i.e. in the Born approximation), the pure Coulomb post form DWBA [Eq. (53)] leads to results which are same as those obtained in a semiclassical model [114]. This agreement is also valid for arbitrary values of η_a and η_c , provided the beam energies are high as compared to the relative energy (E_{cn}) of fragments c and n in the ground state of the projectile. The first order approximation to the amplitude given by Eq. (53), can be written as [114, 115, 61]

$$\hat{\beta}_{\ell m}^{\text{first order}} = 4\pi Z_{\ell m} f_{\text{Coul}} e^{-\frac{\pi}{2}\xi} \times \left[e^{-i\phi} \frac{1}{k_a^2 - [\vec{k}_c + \delta\vec{k}_n]^2} + e^{i\phi} \frac{m_c}{m_a} \frac{1}{k_c^2 - (\delta\vec{k}_n - \vec{k}_a)^2} \right] \quad (81)$$

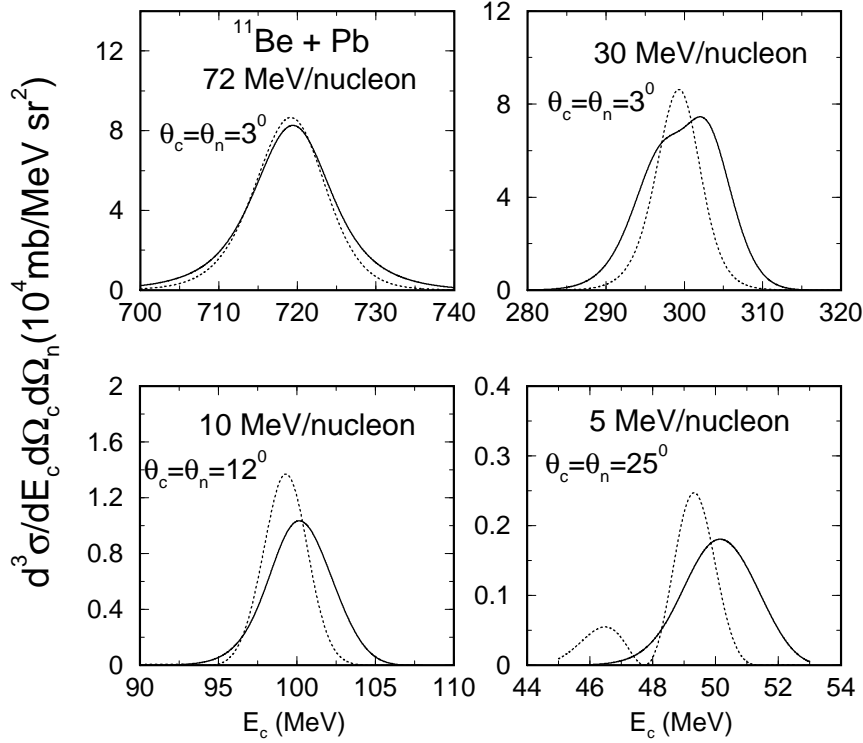


Figure 14: Triple differential cross section as a function of the energy of ^{10}Be core for the reaction $^{11}\text{Be} + \text{Pb} \rightarrow \text{n} + ^{10}\text{Be} + \text{Pb}$ at the beam energies of 72 MeV/nucleon, 30 MeV/nucleon, 10 MeV/nucleon and 5 MeV/nucleon. The results of the finite range DWBA and first-order theory are shown by solid and dotted lines respectively.

where the relative phase $\phi = \sigma(\eta_c) - \sigma(\eta_a) - \sigma(\xi) - \xi/[2 \log |D(0)|]$, with $\sigma(\eta)$ being the usual Coulomb phase shifts, and $\xi = \eta_c - \eta_a$ and $D(0)$ as defined in Eq. (70). In Eq. (81), we have defined $f_{\text{COUL}} = 2\eta_a k_a/k^2$. This term is very similar to the Born approximation (BA) result given in [116]; in the limit $\xi \rightarrow 0$ it actually coincides with the BA expression. This equation can be used to investigate the role of higher order effects (which includes postacceleration). It may be noted that the derivation of Eq. (81) makes use only of the condition $-D(0) \gg 1$ which is met for beam energies large as compared to the binding energy.

We now investigate postacceleration effects in the breakup of the one-neutron halo nuclei ^{11}Be and ^{19}C . We take a heavy target of atomic number $Z=82$. In the following all the higher order results correspond to calculations performed within the finite range post form DWBA theory as discussed in section 3.1. The

structure inputs were also the same as those given their. The first order results have been obtained by using Eq. (81).

In Fig. (14), we present calculations for the triple differential cross sections for the breakup reaction $^{11}\text{Be} + \text{Pb} \rightarrow \text{n} + ^{10}\text{Be} + \text{Pb}$, as a function of the energy of the ^{10}Be core (E_c), for four beam energies lying in the range of 5 MeV/nucleon - 72 MeV/nucleon. To see the postacceleration in a clear way, it is very useful to study the cross-section as a function of the core energy. The results obtained within the higher order and the first order theories are shown by solid and dotted lines, respectively.

It can be seen from this figure that while for lower beam energies, the higher order and first-order results differ considerably from each other, they are almost the same for the beam energy of 72 MeV/nucleon. In each case, the first order cross sections peak at the energy of the core fragment which corresponds to the beam velocity (this value of the core fragment energy will be referred to as E_{bv} in the following). In contrast to this, the peaks of the higher order cross sections are shifted to energies $> E_{bv}$ for the three lower energies. Only for the 72 MeV/nucleon beam energy, does the higher order result peak at E_{bv} . This shows very clearly that the finite range DWBA model exhibits postacceleration for beam energies ≤ 30 MeV/nucleon, while this effect is not present at 72 MeV/nucleon. Therefore, the higher order effects are minimal for the Coulomb breakup of ^{11}Be at the beam energies ≥ 70 MeV. This result is in agreement with those obtained in [113, 62].

In Fig. (15), we compare the results of the first-order and the finite range DWBA calculations for the relative energy spectrum of the fragments emitted in the breakup reaction of ^{11}Be on a ^{208}Pb target for the same four beam energies as shown in Fig. (14). These cross sections have been obtained by integrating over all the allowed values of the angles Ω_{c-n} . In both the models, the integrations over $\theta_{t-(c+n)}$, have been carried out between 1° to grazing angle, in the upper two figures, and between 5° to grazing angles, in the lower two figures. The integrations over $\phi_{t-(c+n)}$ angles have been done over all of its kinematically allowed values. The dotted and solid lines represent the first-order and the higher order results, respectively.

We notice that while for the beam energy of 72 MeV/nucleon, the higher order effects are minimal, they are quite strong for the lower beam energies, being largest at the beam energy of 5 MeV/nucleon. This reinforces the point, already made in [113, 62], that at the beam energy of 72 MeV/nucleon, the higher order effects are quite small if both the first order and the higher order terms are calculated within the same theory.

In Fig. (16), we show the same results as in Fig. (15) but for the ^{19}C induced reaction on the ^{208}Pb target for the beam energies of 67 MeV/nucleon, 30 MeV/nucleon and 10 MeV/nucleon. We see that in this case too the higher order effects are quite weak for the beam energy 67 MeV/nucleon, but appreciable for the lower beam energies.

It may be noted that by comparing the result of the adiabatic model of Coulomb breakup reactions which is conceptually different from ours, with that of the first order semiclassical perturbation theory of the Coulomb excitation, it

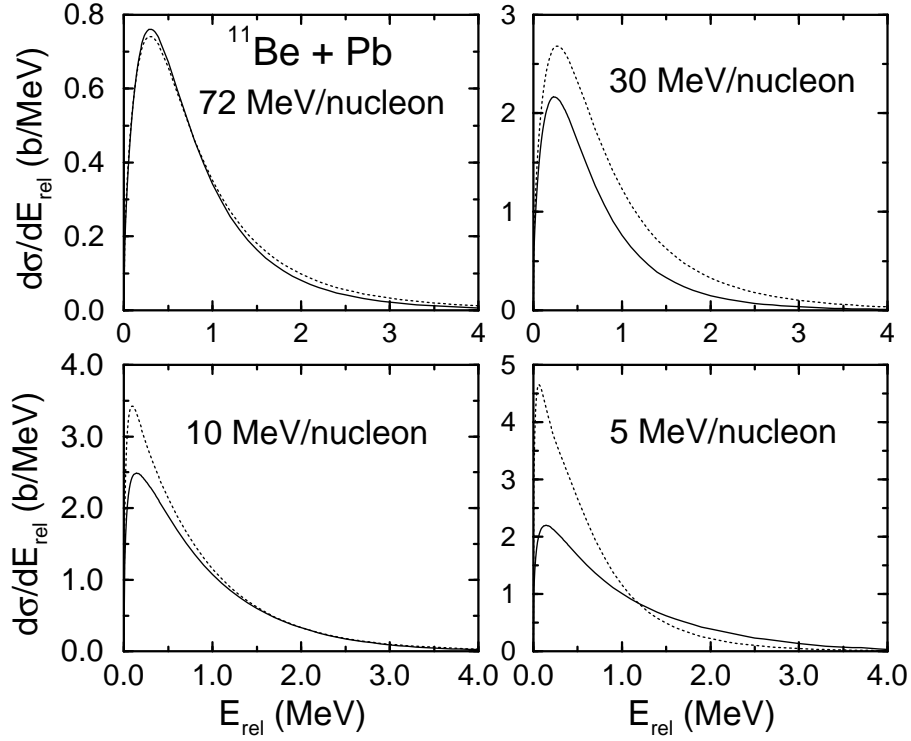


Figure 15: The differential cross section as a function of the relative energy of the fragments (neutron and ^{10}Be) emitted in the ^{11}Be induced breakup reaction on a ^{208}Pb target at the beam energies of 72 MeV/nucleon, 30 MeV/nucleon, 10 MeV/nucleon, and 5 MeV/nucleon. The dotted and full lines represent the first-order and the finite range DWBA results, respectively.

has been concluded in [117] that the higher order effects are substantial for these reactions even at the beam energies ~ 70 MeV/nucleon. However, one should be careful in drawing definite conclusions about the role of the higher order effects from such an approach. For a reliable assessment of the contributions of the higher order effects, it is essential that both the first order and the higher order terms should be calculated within the same theory, as has been done in [113, 62, 115]).

Thus, in the post form DWBA theory, the peaks in the triple and double differential cross sections vs. core energy spectra, are shifted to energies larger than those corresponding to the beam velocity, at the incident energies ≤ 30 MeV/nucleon. Therefore, postacceleration effects are important at these beam energies. On the other hand, at the beam energy ~ 70 MeV/nucleon, the corresponding spectra peak at the beam velocity energies, which is consistent

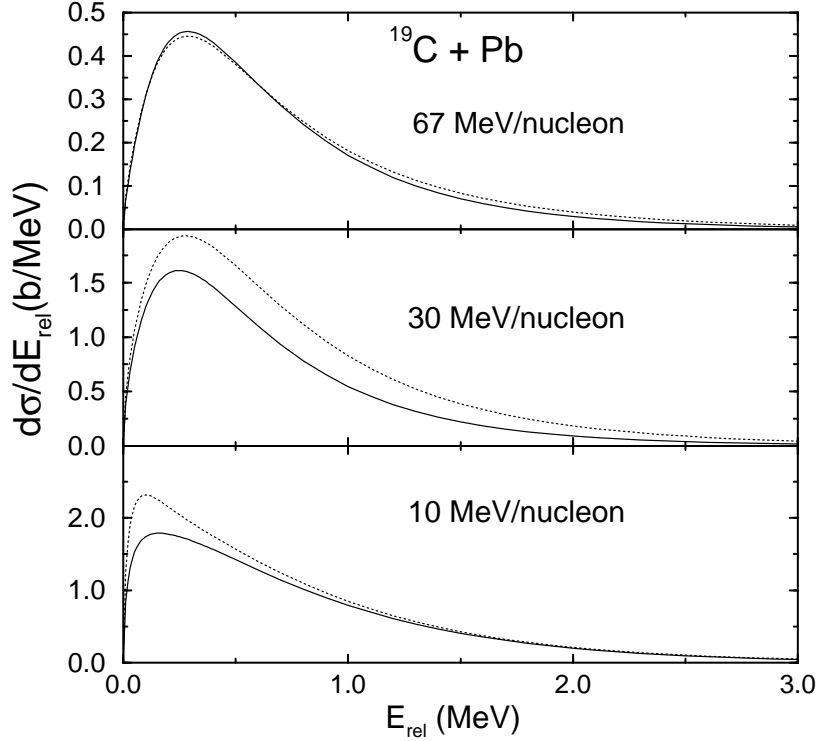


Figure 16: The differential cross section as a function of the relative energy of the fragments (neutron and ^{18}C) emitted in the ^{19}C induced breakup reaction on a ^{208}Pb target at the beam energies of 67 MeV/nucleon, 30 MeV/nucleon, and 10 MeV/nucleon. The dotted and full lines represent the first-order and the finite range DWBA results, respectively.

with no postacceleration. In contrast to this, the first-order cross sections always peak at the beam velocity energy, which is expected as the postacceleration is a higher order effect.

The higher order effects are also found to be quite important in the relative energy spectrum of the fragments at beam energies ≤ 30 MeV/nucleon, while they are insignificant at the beam energies ~ 70 MeV/nucleon. This suggests that the conclusions arrived at in Refs. [90, 112], where the data on the relative energy spectra of the fragments taken in the breakup of ^{11}Be and ^{19}C at beam energies ~ 70 MeV, have been analyzed within the first order theory of the Coulomb excitation, may not be affected by the higher order effects.

It should be noted that from an experimental point of view, the postacceleration effects are not fully clarified (see, e.g., [90, 118, 119]). Finally, let us mention the recent work on the electromagnetic dissociation of unstable neutron-

rich oxygen isotopes [120]. These authors deduce photoneutron cross sections from their dissociation measurements. If the neutrons are emitted in a slow evaporation process in a later stage of the reaction, the question of postacceleration is not there. On the other hand, for the light nuclei there is some direct neutron emission component and the present kind of theoretical analysis further proves the validity of the semiclassical approach used in [120].

Postacceleration effects are also of importance for the use of Coulomb dissociation for the study of radiative capture reactions of astrophysical interest. We expect that our present investigations will shed light on questions of postacceleration and higher order effects in these cases also.

5 Summary, Conclusions and Future Outlook

Due to the potential use of the breakup reactions of neutron rich light exotic nuclei in extraction the information about the structure of these nuclei, it is essential to have a full quantal theory of these reactions which involves minimum number of parameters. To this end, we have developed a theory of one-neutron halo nuclei within the framework of the post form distorted wave Born approximation. Finite range effects of the core-halo interaction are included in this theory which allows the full ground state wave function of the projectile corresponding to any orbital angular momentum structure to enter into this theory. For the one-nucleon halo breakup case, it can treat the Coulomb and nuclear breakups as well as their interference terms within a single framework on an equal footing. Since this theory uses the post form scattering amplitude, the breakup contributions from the entire continuum corresponding to all the multipoles and relative orbital angular momenta of the core-halo system are included in it. This theory can account for the postacceleration effects in a unique way.

Most of the breakup observables are sensitive to the ground state configuration of the projectile. We find that for ^{11}Be , a s - wave configuration [$^{10}\text{Be}(0^+) \otimes 1s_{1/2}\nu$], with a spectroscopic factor of 0.74 for its ground state provides best agreement with the experimental data in all the cases.

We have also performed calculations within an adiabatic model which makes the approximation that the strongly excited core-valence particle relative energies are small in the Coulomb breakup and also within the approximation of Baur and Trautmann which equates the coordinates of the core-target system with those of the projectile-target system. Unlike the DWBA, the adiabatic model does not use the weak coupling approximation to describe the center of mass motion of the fragments with respect to the target. For almost all the observables, there is a general agreement between the DWBA and the adiabatic model results even in the absolute magnitude. However, the approximation of Baur and Trautmann gives results which are very different from those obtained within the DWBA and the adiabatic model.

For the ^{19}C case, the results for the PMD of ^{18}C and the relative energy spectrum of the n - ^{18}C system show that the most probable ground state configuration of ^{19}C is [$^{18}\text{C}(0^+) \otimes 1s_{1/2}\nu$] with a one-neutron separation energy

of 530 keV and a spectroscopic factor of 1. Furthermore, the most probable configuration for ^{15}C is a s – wave valence neutron coupled to the ^{14}C core and that for ^{17}C is a d – wave valence neutron coupled to the ^{16}C core. Both the experimental and the calculated FWHM of the PMD for the ^{14}C core in the breakup of ^{15}C are small and they agree well with each other. This provides support to the existence of a one-neutron halo structure in ^{15}C . On the other hand, in the case of ^{17}C the FWHM of the PMD for the ^{16}C core is closer to that of a stable isotope. Therefore the existence of a halo structure in ^{17}C appears to be unlikely. Interestingly the one-neutron separation energies of ^{15}C and ^{17}C are 1.2181 and 0.729 MeV, respectively. So both the binding energy of the valence neutron as well as its configuration with respect to the core together decide whether a nucleus has halo structure or not.

For medium mass and heavy target nuclei, the neutron angular distributions are dominated by the nuclear and the Coulomb breakup terms at larger and smaller angles, respectively. Contributions of the Coulomb-nuclear interference terms are non-negligible. They can be as big in magnitude as the pure nuclear or the pure Coulomb breakup and have negative or positive sign depending upon the angle and energy of the outgoing fragments. For these targets, the interference terms help in better description of trends of the experimental data even at smaller angles.

In the parallel momentum distribution of the ^{10}Be fragment in the breakup reaction of ^{11}Be , the region around the peak of the distribution, which gets substantial contributions from forward scattered fragments, is Coulomb dominated, while in the wings of the distribution, where contributions come from fragments scattered at large angles, the nuclear breakup contributions dominate. Similarly, the data on relative energy spectra of the fragments (neutron and ^{10}Be) emitted in breakup of ^{11}Be on a heavy target can not be described properly by considering only the pure Coulomb breakup mechanism; inclusion of nuclear and Coulomb-nuclear interference terms is necessary.

In future studies the full quantal theory of the one-neutron halo breakup reactions should be applied to describe the $(a, b\gamma)$ reaction. The data for these reactions [121, 122] taken at the Michigan State University are yet to be described within a full quantal reaction model. Since, the relevant partial cross sections of the core fragments are essentially inclusive, both elastic and inelastic breakup modes will contribute to them. Our theory can be extended to calculate the latter mode in a straight forward manner. In fact all the ingredients required for this extension have already been calculated by us.

There is also a need to extend the theory to describe the halo breakup at higher beam energies for which data have been taken at GSI, Darmstadt. This can be achieved by introducing the eikonal expansion of the distorted waves, instead of the partial wave expansion as done in section 3.2.

Our theory should be used to analyze the breakup data of ^8B on a ^{58}Ni target at the beam energy of 25.8 MeV. At this energy the nuclear breakup effects are quite strong and the Coulomb-nuclear interference terms should manifest themselves in an important way. It should be noted that in the CDCC model analysis of these data, the continuum states corresponding to much larger excita-

tion energies and relative orbital angular momenta were required to be included in order to get a proper convergence. Our post form breakup theory includes, by its very construction, contributions from the entire continuum corresponding to all the excitation energies, multipoles and relative orbital angular momenta of the core-valence nucleon system. Therefore, a comparison of our calculations with these data would be interesting also from the point of view of checking and supplementing the corresponding CDCC results.

The study of the ${}^8\text{Li}(\alpha, n){}^{11}\text{B}$ reaction is of crucial importance in determining the abundance of ${}^{11}\text{B}$, since nuclides with $A \geq 12$ pass through ${}^{11}\text{B}$ on their way to higher masses. However, the α -capture reaction ${}^8\text{Li}(\alpha, n){}^{11}\text{B}$ is in competition with the ${}^8\text{Li}(n, \gamma){}^9\text{Li}$ reaction which turns the reaction flow back to lighter elements via ${}^9\text{Li}(\beta^-, \nu){}^9\text{Be}(p, \alpha){}^6\text{Li}$. Thus the cross sections of these reactions are extremely important in predicting the yields of elements with $A \geq 12$. We would like to apply our theory to investigate the breakup reaction ${}^9\text{Li} \rightarrow {}^8\text{Li} + n$ on a heavy target like ${}^{208}\text{Pb}$. It would be interesting to know how far the data taken recently at the Michigan State University can be described solely by the Coulomb breakup mechanism and what is the role of the nuclear breakup effects in these data. This is important as the pure Coulomb breakup cross sections for this reaction can be used to extract the cross sections for the reverse reaction ${}^8\text{Li}(n, \gamma){}^9\text{Li}$.

The authors would like to express their thanks to P. Banerjee, G. Baur, P. Danielewicz and H. Lenske for several useful discussions on the present topic.

References

- [1] P. G. Hansen and B. M. Sherill, Nucl. Phys. A **693** (2001) 133.
- [2] White Paper: Scientific Opportunities with Fast Fragmentation Beams from RIA, NSCL, Michigan State University, 2000.
- [3] I. Tanihata, Nucl. Phys. A **654** (1999) 235c.
- [4] B. Jonson, Nucl. Phys. A **631** (1998) 376c.
- [5] White Paper for the ‘‘Columbus’’ Workshop: Scientific Opportunities with an Advanced ISOL facility, 1997.
- [6] I. Tanihata, J. Phys. G **22** (1996) 157.
- [7] P. G. Hansen, A. S. Jensen and B. Jonson, Ann. Rev. Nucl. Part. Sci. **45** (1995) 591.
- [8] K. Riisager, Rev. Mod. Phys. **66** (1994) 1105.
- [9] M. V. Zhukov, B. V. Danilin, D. V. Federov, J. M. Bang, I. J. Thompson and J. S. Vaagen, Phys. Rep. **231** (1993) 151.
- [10] C. A. Bertulani, L. F. Canto and M. S. Hussain, Phys. Rep. **226** (1993) 281.

- [11] P. G. Hansen, Nucl. Phys. A **553** (1993) 89c.
- [12] A. C. Mueller and B. M. Sherill, Ann. Rev. Nucl. Part. Sci. **43** (1993) 529.
- [13] S. M. Austin and G. F. Bertsch, Scientific American (June, 1997) 62; P. G. Hansen, New Scientist (Oct. 9, 1993) 38.
- [14] A. C. C. Villari, Nucl. Phys. A **693** (2001) 465c.
- [15] I. Tanihata *et al.*, Phys. Rev. Lett. **55** (1985) 2676; I. Tanihata *et al.*, Phys. Lett. B **206** (1988) 592.
- [16] W. Mittig *et al.*, Phys. Rev. Lett. **59** (1987) 1889.
- [17] M. G. Saint-Laurent *et al.*, Z. Phys. A **332** (1989) 457.
- [18] M. Fukuda *et al.*, Phys. Lett. B **268** (1991) 339.
- [19] D. Cortina-Gil *et al.*, Eur. Phys. J. A **10**, 49 (2001).
- [20] R. Kanungo *et al.*, Phys. Rev. Lett. **88**, 142502 (2002).
- [21] E. H. S. Burhop, D. H. Davis, J. Sacton and G. Schorochoff, Nucl. Phys. A **132** (1969) 625.
- [22] M. Fukuda *et al.*, Phys. Lett. B **268** (1991) 339.
- [23] D. Bazin *et al.*, Phys. Rev. C **57** (1998) 2156.
- [24] V. Guimarães *et al.*, Phys. Rev. C **61** (2000) 064609.
- [25] D. Bazin. *et al.*, Phys. Rev. Lett. **74** (1995) 3569.
- [26] I. Tanihata *et al.*, Phys. Lett. B **160** (1985) 380.
- [27] I. Tanihata *et al.*, Phys. Lett. B **287** (1992) 307.
- [28] T. Suzuki *et al.*, Nucl. Phys. A **658** (1999) 313.
- [29] M. Labiche *et al.*, Phys. Rev. Lett. **86** (2001) 600.
- [30] M. H. Smedberg *et al.*, Phys. Lett. B **452** (1999) 1.
- [31] M. Fukuda *et al.*, Nucl. Phys. A **656** (1999) 209.
- [32] V. Guimarães *et al.*, Phys. Rev. Lett. **84** (2000) 1862.
- [33] A. Ozawa *et al.*, Phys. Lett. B **334** (1994) 18.
- [34] T. Suzuki *et al.*, Nucl. Phys. A **616** (1997) 286c.
- [35] A. Navin *et al.*, Phys. Rev. Lett. **81** (1998) 5089.
- [36] R. Serber, Phys. Rev. **72** (1947) 1008.

- [37] G. Baur, F. Rösler, D. Trautmann and R. Shyam, Phys. Rep. **111** (1984) 333.
- [38] M. Gell-Mann and M. L. Goldberger, Phys. Rev. **91** (1953) 398.
- [39] F. S. Levin, Ann. Phys. **46** (1968) 1.
- [40] C. M. Vincent, Phys. Rev. **175** (1968) 1309.
- [41] G. R. Satchler, *Direct Nuclear Reactions*, Oxford University Press, New York, 1991.
- [42] R. Huby and J. R. Mines, Rev. Mod. Phys. **37** (1965) 406.
- [43] G. Baur and D. Trautmann, Nucl. Phys. A **199** (1973) 218; Phys. Rep. **25** (1976) 293; G. Baur, F. Rösler and D. Trautmann, Nucl. Phys. A **265** (1976) 101; G. Baur, R. Shyam, F. Rösler and D. Trautmann, Helv. Phys. Acta **53** (1980) 506.
- [44] J. Pampus *et al.*, Nucl. Phys. A **311** (1978) 141; J. Kleinfeller *et al.*, Nucl. Phys. A **370** (1981) 205.
- [45] R. Shyam, P. Banerjee and G. Baur, Nucl. Phys. A **540** (1992) 341; P. Banerjee and R. Shyam, Nucl. Phys. A **561** (1993) 112; Phys. Lett. B **318** (1993) 268.
- [46] F. Rybicki and N. Austern, Phys. Rev. C **6** (1972) 1525; H. Amakawa and N. Austern, Aust. J. Phys. **36** (1983) 633; N. Austern, Phys. Rev. C **30** (1984) 1130; M. Yahiro, Y. Iseri, M. Kamimura and M. Nakano, Phys. Lett. B **141** (1984) 19.
- [47] R. Shyam and I. J. Thompson, Phys. Rev. C **59** (1999) 2645.
- [48] K. Alder and A. Winther, *Electromagnetic Excitation*, North-Holland Publishing Co., Amsterdam, 1975.
- [49] M. Kamimura *et al.*, Prog. Theor. Phys. Suppl. **89** (1986) 1.
- [50] G. Baur R. Shyam, F. Rösler and D. Trautmann, Phys. Rev. C **28** (1983) 946.
- [51] F. M. Nunes and I. J. Thompson, Phys. Rev. C **59** (1999) 2652.
- [52] J. A. Tostevin, F. M. Nunes and I. J. Thompson, Phys. Rev. C **63** (2001) 024617.
- [53] J. Mortimer, I. J. Thompson and J. A. Tostevin, Phys. Rev. C **65** (2002) 064619.
- [54] A. N. Moro, R. Crespo, F. Nunes and I. J. Thompson, Phys. Rev. C **66** (2002) 024612.

- [55] G. Baur, Z. Physik A **277** (1976) 147.
- [56] R. Shyam, G. Baur, F. Rösler and D. Trautmann, Phys. Rev. C **19** (1979) 1246.
- [57] H. Esbensen, G. F. Bertsch and C. A. Bertulani, Nucl. Phys. A **581** (1995) 107; G.F. Bertsch, K. Hencken, and H. Esbensen, Phys. Rev. C **57**, 1366 (1998); H. Esbensen and G.F. Bertsch, Phys. Rev. C **59**, 3240 (1999).
- [58] V. S. Melezhik and D. Baye, Phys. Rev. C **59** (1999) 3232.
- [59] A. Bonaccorso and F. Carstoiu, Phys. Rev. C **61**, 034605 (2000) and references therein.
- [60] K. Yabana, Y. Ogawa and Y. Suzuki, Nucl. Phys. A **539**, 295 (1992).
- [61] G. Baur, K. Hencken and D. Trautmann, nucl-th/0304041.
- [62] S. Typel and R. Shyam, Phys. Rev. C **64** (2001) 024605.
- [63] R. Chatterjee and R. Shyam, Phys. Rev. C **66** (2002) 061601(R).
- [64] R. Chatterjee, Phys. Rev. C **68** (2003) 044604.
- [65] J. Margueron, A. Bonaccorso, and D. M. Brink, Nucl. Phys. A **703** (2002) 105; Nucl. Phys. A **720** (2003) 337.
- [66] L. F. Canto, R. Donangelo, A. Romanelli and H. Schulz, Phys. Lett. B **318** (1993) 415; C. A. Bertulani, L. F. Canto and M. S. Hussein, Phys. Lett. B **353** (1995) 413.
- [67] T. Kido, K. Yabana and Y. Suzuki, Phys. Rev. C **50** (1994) R1276; **53** (1996) 2296.
- [68] G. F. Bertsch and C. A. Bertulani, Nucl. Phys. A **556** (1993) 136; C. A. Bertulani and G. F. Bertsch, Phys. Rev. C **49** (1994) 2839.
- [69] P. G. Hansen *et al.*, Phys. Rev. Lett. **77** (1996) 1016.
- [70] R. Anne *et al.*, Nucl. Phys. A **575** (1994) 125.
- [71] C. A. Bertulani, G. Baur and M.S. Hussein, Nucl. Phys. A **526** (1991) 751.
- [72] P. Braun-Munzinger and H. L. Harney, Nucl. Phys. A **233** (1974) 381.
- [73] P. Braun-Munzinger, H. L. Harney and S. Wenneis, Nucl. Phys. A **236** (1974) 190.
- [74] R. Shyam and M.A. Nagarajan, Ann. Phys. (NY) **163**, 285 (1985).
- [75] G. Baur and D. Trautmann, Nucl. Phys. A **191** (1972) 321.

- [76] R. Shyam, P. Banerjee and G. Baur, Nucl. Phys. A **540** (1992) 341.
- [77] R. Chatterjee, P. Banerjee and R. Shyam, Nucl. Phys. A **675** (2000) 477.
- [78] P. Banerjee, I. J. Thompson and J. A. Tostevin, Phys. Rev. C **58** (1998) 1042.
- [79] F. M. Nunes, I. J. Thompson and R. C. Johnson, Nucl. Phys. A **596** (1996) 171.
- [80] D. L. Auton, Nucl. Phys. A **157** (1970) 305.
- [81] B. Zwieglinski, W. Benenson, and R. G. H. Robertson, Nucl. Phys. A **315** (1979) 124.
- [82] J. A. Tostevin, S. Rugmai and R. C. Johnson, Phys. Rev. C **57** (1998) 3225; J. A. Tostevin *et al.*, Phys. Lett. B **424** (1998) 219
- [83] R. C. Johnson, J. S. Al-Khalili and J. A. Tostevin, Phys. Rev. Lett. **79** (1997) 2771.
- [84] J. A. Christley, J. S. Al-Khalili, J. A. Tostevin and R. C. Johnson, Nucl. Phys. A **624** (1997) 275.
- [85] R. C. Johnson, J. Phys. G: Nucl. & Part. Phys. **24** (1998) 1583.
- [86] H. Fuchs, Nucl. Instrum. Methods **200** (1982) 361; G. G. Ohlsen, Nucl. Instrum. Methods **37** (1965) 240.
- [87] A. Nordsieck, Phys. Rev. **93** (1954) 785.
- [88] P. Banerjee and R. Shyam, Phys. Lett. B **318** (1993) 268; J. Phys. G **22**, L79 (1996).
- [89] H. Lenske, J. Phys. G: Nucl. & Part. Phys. **24** (1998) 1429.
- [90] T. Nakamura *et al.*, Phys. Lett. B **331** (1994) 296.
- [91] C. H. Dasso, S. M. Lenzi and A. Vitturi, Nucl. Phys. A **539** (1999) 59.
- [92] N. A. Orr *et al.*, Phys. Rev. C **51** (1995) 3116.
- [93] J. H. Kelley *et al.*, Phys. Rev. Lett. **74** (1995) 30.
- [94] D. Bazin *et al.*, Phys. Rev. Lett. **74** (1995) 3569; Phys. Rev. C **57** (1998) 2156.
- [95] C. A. Bertulani and K. W. McVoy, Phys. Rev. C **46** (1992) 2638.
- [96] P. Banerjee and R. Shyam, Phys. Lett. B **349** (1995) 421.
- [97] P. Banerjee and R. Shyam, Phys. Rev. C **61** (2000) 047301.

- [98] D. Ridikas, M. H. Smedberg, J. S. Vaagen and M. V. Zhukov, *Europhys. Lett.* **37** 385 (1997); *Nucl. Phys. A* **628** 363 (1998).
- [99] Z. Ren, Z. Y. Zhu, Y. H. Cai and G. Xu, *Nucl. Phys. A* **605** (1996) 75.
- [100] Angela Bonaccorso, *Phys. Rev. C* **60** (1999) 054604.
- [101] V. Maddalena and R. Shyam, *Phys. Rev. C* **63** (2001) 054608.
- [102] U. Datta Pramanik *et al.*, *Phys. Lett. B* **551**, 63 (2003).
- [103] C.M. Vincent and H.T. Fortune, *Phys. Rev. C* **2**, 782 (1970).
- [104] R. Chatterjee, Ph.D. Thesis, Jadavpur University, Kolkata (2003).
- [105] C.M. Perey and F.G. Perey, *Atomic Data and Nuclear Data Tables* **17**, 1 (1976).
- [106] M. Beunard *et al.*, *Nucl. Phys. A* **424**, 313 (1984).
- [107] J.H. Kelley *et al.*, *Phys. Rev. Lett.* **74**, 30 (1995).
- [108] G. Baur and D. Trautmann, *Nucl. Phys.* **A191**, 321 (1972).
- [109] G. Baur, C. A. Bertulani, and D. M. Kalassa, *Nucl. Phys. A* **550**, 107 (1995).
- [110] G. Baur and D. Trautmann, *Phys. Rep.* **25C**, 293 (1976).
- [111] P. Banerjee and R. Shyam, *Nucl. Phys.* **A561**, 112 (1993).
- [112] T. Nakamura *et al.*, *Phys. Rev. Lett.* **83** (1999) 1112.
- [113] S. Typel and G. Baur, *Phys. Rev.* **C64**, 024601 (2001).
- [114] G. Baur, K. Hencken, and D. Trautmann, LANL preprint nucl-th/0108013.
- [115] P. Banerjee, G. Baur K. Hencken, R. Shyam and D. Trautmann, *Phys. Rev. C* **65** (2002) 064602.
- [116] G. Baur, K. Hencken, D. Trautmann, S. Typel, and H.H. Wolter, *Prog. in Part. and Nucl. Phys.* **46**, 99 (2001).
- [117] J.A. Tostevin, *Proceedings of the Second International Conference on Fission and Properties of Neutron-rich Nuclei*, St. Andrews, Scotland, June 28 - July 2, 1999, edited by J. H. Hamilton, W. R. Phillips and H. K. Carter, World Scientific, Singapore (2000), 429.
- [118] K. Ieki *et al.*, *Phys. Rev. Lett.* **70** (1993) 730.
- [119] J. E. Bush *et al.*, *Phys. Rev. Lett.* **81** (1998) 61.

- [120] A. Leistenschneider et al., Phys. Rev. Lett. **86**, 5442 (2001).
- [121] A. Navin *et al.*, Phys. Rev. Lett. **85** (2000) 266.
- [122] V. Maddalena *et al.*, Phys. Rev. C **63** (2001) 024613.